AN ABSTRACT OF THE DISSERTATION OF

Ganesh Gore for the degree of Master of Science in
Electrical and Computer Engineering presented on June 28, 2006.

Title: Scaled modeling and Simulation of Ocean Wave Linear Generator Buoy Systems

Abstract approved:_____

Annette R. von Jouanne

Accurate scaled modeling and simulation are critical to advancing ocean wave linear generator buoys. A 100^{th} scaled model of ocean wave generator buoy systems is analyzed by solving the Navier-Stokes equations. These equations are numerically solved using Computational Fluid Dynamics (CFD) by implementing the front capturing method. In this thesis, winter and summer wave profiles are considered and the heave velocity of an oscillating buoy is studied in order to predict and to understand the power generated by the buoy. The results from the CFD simulations need to be compared with experimental data, thus a wave flume design from a dimensions perspective is presented. In addition, a 100^{th} scaled permanent magnet linear generator design for high efficiency is presented.

The ocean buoy design is presented by drawing the transfer function in the heave motion. The frequency domain analysis is overlapped on the wave energy spectra for summer climate condition. MATLAB program scripts are listed for

buoy sizing and linear generator design. The linear generator design is verified using Maxwell-2D Finite Element Modeling (FEM) code.

From simulations, it was found that given the diameter of the ocean buoy of 4.5m, it can generate 24 kW rms power in winter, however the buoy can only generate 3.3kW rms power in summer considering a damping factor of 0.25.

The optimized design of the PM linear generator designed using a 1mm air gap, with an efficiency of 96.5%, produces 2.2 W with a peak thrust of 30 N.

The damped frequency of heave motion is plotted and it is found that a 4.5m diameter buoy produces heave motion in the frequency range of the high energy spectrum.

Scaled modeling and Simulation of Ocean Wave Linear Generator Buoy Systems

By
Ganesh P Gore

A THESIS

Submitted to

Oregon State University

in partial fulfillment of
the requirements for the
Degree of

Master of Science

Presented June 28, 2006
Commencement June 2007

Master of Science dissertation of Ganesh P. Gore presented on June 28, 2006.

APPROVED:

Major Professor, representing Electrical and Computer Engineering

---

Director of the School of Electrical Engineering and Computer Science

---

Dean of the Graduate School

I understand that my dissertation will become part of the permanent collection of Oregon State University libraries. My signature below authorizes release of my dissertation to any reader upon request.

Ganesh P Gore

ACKNOWLEDGEMENTS

I would like to express my deepest gratitude to Dr. von Joanne for her guidance, advice, and encouragement. It has been a privilege to conduct this research under her supervision. I am thankful to the late Dr.Wallace who gave valuable suggestions during discussion meetings.

I would also like to thank Dr. Molly Shor, Dr. Huaping Liu and Dr. David Hackleman for their helpful suggestions.

Special thanks go to Ken Rhinefrank, Emmanuel Agamloh and all of the wave energy team for the fruitful discussions in carrying out this research.

Thanks also go to my friend Jameel Ahamad for valuable discussions about the signal processing tool box.

Finally, I am thankful to my family, whose support, love and patience truly made this research possible.

Ganesh Gore

Graduate Student, ECE

DEDICATION

To my dear late father Pandurang Shankarao Gore

TABLE OF CONTENTS

TABLE OF CONTENTS (Continued) Page

LIST OF FIGURES

LIST OF FIGURES (Continued)

LIST OF TABLES

LIST OF APPENDICES

LIST OF ACRONYMS

OWEC	Ocean Wave energy converter.
g	Acceleration due to gravity, m/s^2
ρ	Density of water, kg/m^3
a	Wave magnitude, m
H	Wave height m
T	Wave period, sec
ω	Wave frequency, rad /s
$\lambda = \frac{2\pi g}{\omega^2}$	Wave length
P	Wave power per unit width, k W/m
$\frac{\lambda}{2\pi}$	Ideal OWEC power capture width in heave, m
V_{ol}	Displaced volume of water, m^3
$m = \rho V_{ol}$	Dry mass, kg
m'	Mass of entrained water, kg
$m_v = m + m'$	Effective mass of OWEC , kg
b	Hydrodynamic damping coefficient, kNs/m
$De = b_{pto} + b$	Effective damping of OWEC, kNs/m
$p(t)$	Instantaneous power converted, kW
P_{mean}	Mean power converted, kW
PMLG	Permanent Magnet Linear Generator.
Taup	Magnet Length

Tau	Pole pitch
Tauslot	Slot Pitch
hm	Magnet ring height
hsu	Slot Depth
ts	Slot Opening
Im	Current from Generator
El	Emf Generated in PMLG
F_{pk}	Peak Thrust
d	Diameter of float (buoy)
A	Wave Amplitude
A_t	Amplitude of Transmitted Wave
n_c	Number Of Conductors
K_{fill}	Fill factor for coils
J_o	Exciting Current in Coil
μ_0	Permeability of Free Space
v	Magnetic Potential
M	Magnetization Vector
B_n	Normal Flux Density to integral surface
B_t	Tangential Flux Density to integral surface
z	position of translator

Φ	Flux Passing Through Each Turn in Time t
N	No of Turns in Coil
f_n	Normal force
f_t	Tangential Force
C_D	The drag coefficient for the buoy
A_N	The projection in a plane normal to the flow, of the buoy
V	Water velocity
X	Heave
S	Pole cross section area
D	Draft
σ	Phase angle between force and wave
η_0	Wave surface expression
D	Damping coefficient
F	Body force
t	Time

SCALED MODELING AND SIMULATION OF OCEAN WAVE LINEAR GENERATOR BUOY SYSTEMS.

CHAPTER 1. INTRODUCTION

1.1 Introduction

Renewable energy sources are only 9% of the world's total power generation [1]. Most of the world's energy is supplied by natural or conventional forms of energy (nuclear, coal and natural gas). As these conventional sources have limited life, energy conversion technologies such as wind turbines and ocean power converters are continuously being investigated. A vast source of ocean wave power is so far untapped because of random and severe variations in ocean waves.

Ocean waves are created when the wind blows over the ocean. Once the energy is transformed to waves, waves travel several miles with little loss of energy. The intensity of waves can be predicted several days before their arrival.

The wave height, wave period and depth of water are three parameters which form the wave climate. These parameter variations must be carefully studied before designing the OWEC (Ocean wave energy converter) systems. Further the extreme values are important in designing reliable OWEC systems. Moreover advanced control systems, needed to tune devices at various frequencies can be developed based on the wave climate. It can be observed that the wave climate follows a cyclic change and wave power in summer is 6 times lower than in winter [2].

1.2 Energy and power density

The energy density of waves is the energy flux crossing the plane parallel to the wave crest. The power density is defined as energy density over the period and is given by [3].

$$P = \frac{1}{32\pi} * \rho * g^2 * T * H^2 \tag{1.1}$$

$$P = 0.42 * T * H^2 \quad [4] \tag{1.2}$$

Equation (1.2) is obtained from the Bret Schneider spectrum with conditions suitable to the Oregon coast [4].

For the Oregon coast, the average power per width is taken as 21.2 kW/m of crest length [4]. In explaining benefits of ocean power over land, OPT says

"The footprint of a 100 MW conventional power plant superstructure, including surrounding grounds, fuel unloading areas, waste settling ponds, and additional facilities can require up to 2 square miles of valuable real estate. A comparable OPT power plant would occupy less than 1 square mile of unused ocean surface out of sight from the shore" [5].

The total average wave energy of US coastline is calculated as 2100 x 10^{12} WH [4], if the water depth of 60 m is considered. It can supply 10 % of the total energy demand of US at 50% efficiency. In the following section we will consider a few currently deployed OWEC systems.

1.3 Literature Review of OWEC systems.

Many OWEC devices, deployed in ocean waves, are the commercially fully functioning devices or at the stage of final testing. However other devices are at the stage of verifying functionality. In this part only the devices which are fully functioning and prototype tested at least once are considered.

1.3.1 Pelamis (OPD) [Category: attenuator]

This device consists of floating cylindrical sections linked by hinged joints (4-5). The wave induces relative motion between these sections. This relative motion is restricted by hydraulic rams. These use hydraulic rams to pump high pressure oil through hydraulic motors. The motors drive electrical generators to produce electricity. A full scale 4 segment prototype 750 kW was successfully tested in 2004. The company is using hydraulics because of good industrial knowledge availability about the system and the cost of manufacturing is low. However the drawback of the system could be maintenance and operational cost. Also there is risk of environmental pollution and hazard in case the oil leaks into the sea water. The EPRI wave energy feasibility project has selected the Pelamis as one of the technologies for assessment. Oregon (21.2 kW/m) is selected as site for evaluation. Please refer to fig. 1.1.

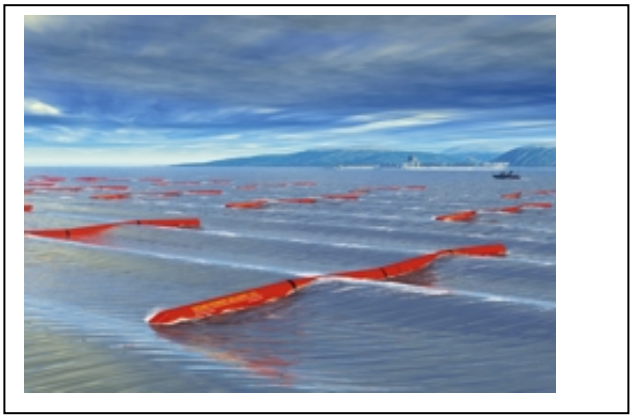

Figure 1.1 Pelamis OWEC devices

1.3.2 Energetech [category: Terminator OWC]

Energetech has built an OWC type of device. In this type of device when the wave approaches the device, it forces air above it into the air chamber, whereas, when the wave retreats, it pulls out air from the chamber. The air chamber is connected to turbine. A full scale 500 kW prototype is built by Energetech, undergoing testing at Port Kembla in Australia [6]. Please refer to fig. 1.2.

Figure 1.2 Energetech OWEC device

1.3.3 Wave Dragon [category: Overtopping devices]

These types of devices have reservoirs. The waves roll into reservoir. The released water from reservoir is used to drive hydro-turbines. Due to long length, these types of devices are placed near shore and special locations are needed to be found for these devices. Wave dragon has deployed 7 MW demonstration project off the coast of Wales. Please refer to fig. 1.3.

Figure 1.3 Wave Dragon OWEC device

1.3.4 Wave swing [Category: bottom mounted point absorber]

The AWS wave energy converter consists of the wave crest and trough, to compress and expand the air inside cylinder to balance pressure. This causes relative movement between the floater and basement. This relative movement drives the generator. A 2 MW rated capacity AWS system has been deployed off Portugal and successfully tested. The device needs to be installed below sea water at a depth of 80-90 meters. The advantage of below water deployment is that the

device is safe from extreme wave conditions. However the installation cost is very high. Please refer to fig. 1.4.

Source http://www.waveswing.com/

Figure 1.4 Wave Swing OWEC device

1.3.5 Aqua Buoy [category: floating point absorber]

In this OWEC device, the heave motion of buoy is coupled to a piston. The movement of piston elongates and releases hose, containing sea water, acting as a pump. The pressurized fluid can be used to drive turbine. A 1 MW pilot offshore demonstration power plant is developed at Makah bay, Washington. Please refer to fig. 1.5.

Figure 1.5 Aqua Buoy OWEC device

1.3.6 Direct drive PMLG buoy (category: floating point absorber)

This project is developed by Oregon State University (OSU). A floating buoy heaves with ocean waves. The float contains an armature. The magnets are mounted on a spar. The spar is slack moored and damping plates are provided to keep it stationary. The relative motion between float and spar is utilized to generate power. The prototype was designed and tested in a wave flume in 2004. If the design challenges of keeping the spar stationary in random waves and controlling heave motion of the buoy in changing wave climates are met, then this technology may be a good competitor in ocean wave converter designs.

The system is very stable as there are no rotating parts, low maintenance cost as the buoy is floating and the principle is simple. To improve the efficiency of machine, transverse and radial flux machines are under study at OSU. The device

needs special protection from severe wave conditions, and can be designed to be winched under in extreme wave conditions. Please refer fig. 1.6.

Source www.oregonstate.edu

Figure 1.6 PMLG OWEC system.

1.3.8 CTFS direct driven OWEC [category: floating point absorber]

This is another project developed by OSU. In this project the iron buoy heaves in ocean waves. This causes linear motion of a spar mounted ball screw. The linear motion of the ball screw is coupled to a shaft and the shaft rotates a generator thereby producing power. The unidirectional clutch keeps the shaft moving in one direction. The advantages of this system are contact-less force transmission (float and magnetic piston/ball screw); high efficiency of ball screw runs the generator at a very high speed. The system is tested in a monochromatic

wave flume in 2005. The response of the system in random waves is yet to be tested. It would be of particular interest to see how the rotary system operates in vibrational environment of the sea. Again the challenges of PMLG described earlier are applicable to CTFS OWEC system as well. Please refer to fig. 1.7.

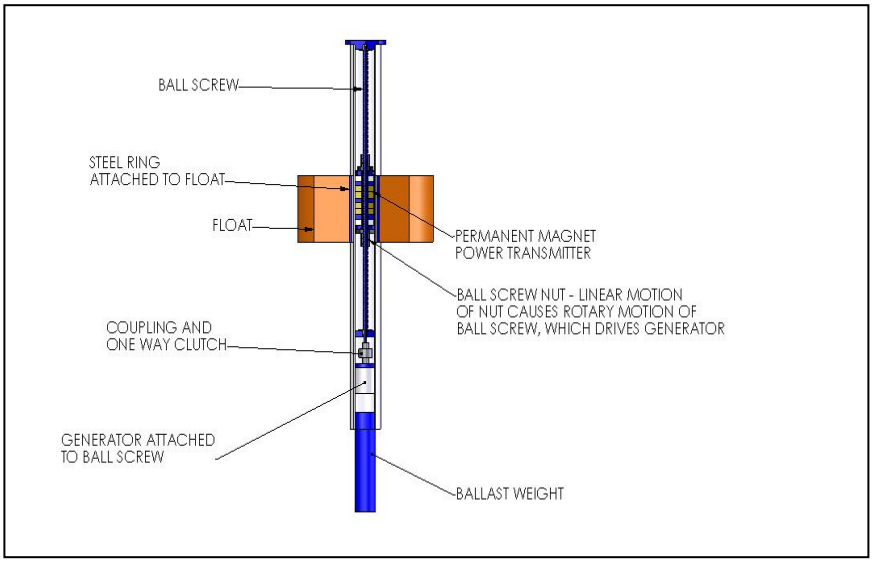

Figure 1.7 CTFS direct driven OWEC

1.4 Environmental impact

Wave energy converters pose several environmental risks. The major effect is on sea life and ship navigation [7]. The wave energy development community needs to address and solve these problems for the benefit of the society. In this section only the environmental impact applicable to point absorbers is discussed.

1.4.1 Environmental effect on sea creatures

The noise emission below and above the sea water must be kept within certain acceptable limits. The devices must be protected to avoid sea creature's contact. The electromagnetic fields and vibrations have effect on mammal sonar and fish reproduction. Mitigation techniques must be developed.

The wave intensity at shoreline might get decreased due to near shore devices. This could be a problem for surfers. So OWEC deployment sites must be selected away from public ocean areas.

1.4.2 Economic consideration

The cost estimate of electricity after testing commercial scaled converters in Oregon site is $0.09 to $0.11/kWh [4]. These sites are high energy density sites. The study is conducted by EPRI. Recent study shows the cost estimates are going up to $0.25 /kWh for Oregon coast. Since the technology is at premature stage, after commercial success, the rates will be clearer.

1.5 Numerical Computation versus Experimental Studies

The ocean wave study can be simulated by using commercially available software in the field of CFD. The software tries to solve non-linear Navier-stroke equations and tries to resolve forces based on Newton's second law of motion. The issues which are of particular interest are accuracy of parameters, integration algorithms and complexity of design and computational intensive resources.

The computational time required to solve the problem is very high. Moreover it is very difficult to model specifics of power take off systems, considering general CFD code. Also dynamic pressure, mooring of buoy etc. can not be modeled in CFD. The solution obtained remains an estimate, and not an actual solution.

In response to these problems, an alternative small wave flume system is designed. The purpose of this system is to test scaled models by changing wave climate. The flume is completely programmable. So wave height, period can be instantaneously changed, and also the water depth. The scaled OWEC systems important features like the power take off system, the power generation capability and efficiency can be tested. Moreover time to get the results is very fast. Since the flume contains sea water, issues such as mooring, dynamic pressure will be taken care of. Moreover these parameters can be measured and plugged into CFD code so that CFD models can be corrected.

The major issue in using these models is scaling factors. All physical quantities must be properly scaled in a scaled environment. Also the issue of wave forces and surface tension must be studied in the scaled environment to see if they are comparable with actual environment.

This thesis is a very preliminary step to answer some of the following questions. However many of the issues will be resolved after designing the wave flume.

First a high capacity, OWEC device, to test at various wave climates is built. This will help to resolve sizing issues for various wave climates. Also for such a small model, if designed materials (properties) are not available, then the efficiency might be low, so high capacity is inevitable.

The experiment on an actual flume will help to determine what capacity factor is optimal for a given site. Considering the randomness of ocean waves, the

goal is to develop a sophisticated algorithm for optimization of capacity factor for the changing wave climate.

The flume will help to understand the scaled operational and maintenance cost of OWEC devices, if operated for a long time.

Efficiency of converting wave power into electric power is to be determined in two stages. Stage one is converting wave power to drive the armature of a PMLG. The stage-two efficiency is to convert thrust into rated power. This is particularly the PMLG efficiency itself.

A final question is regarding the devices described above, and that is which technology will yield the optimum economics?

1.6 Thesis Outline

The scaled model of a prototype is considered for design. Chapter 2 explains CFD modeling. First governing CFD equations are explained. Then the specifics of CFD grid, integration method, boundary conditions are explained. Finally an example with summer wave climate at the Oregon coast is considered and power developed by the buoy is shown with CFD simulated results.

In the next chapter, the wave flume design is explained. The particular approach is to explain the dimensions selected for the flume. The wave maker, wave length issues and the separation between buoys is explained. The scaling factors for various dimensions are presented. Then, the actual experimental setup and instrumentation is explained, very briefly.

In chapter no 3, the complete design of the PMLG generator is explained. The appendix lists the MATLAB code. The readers are suggested to read [8] for

understanding of equations involved. The design is optimized for various parameters. Finally the design is verified using Maxwell 2D FEM code.

In the final chapter, the procedure to design a full scaled prototype is explained. The heave motion transfer function is super-imposed on the wave spectra to understand the frequency of the oscillating buoy in presence of high energy content frequencies. The Bret Schneider spectrum is developed for summer profile.

The thesis ends with conclusions and future work.

CHAPTER 2. CFD ANALYSIS OF HEAVE MOTION OF BUOY.

2.1 Introduction

This chapter begins with basic terms related to ocean waves followed by an explanation of linear wave theory. The properties of waves are mathematically formulated. The boundary conditions are explained. Then energy transfer by progressive waves is explained very briefly. The equation for power produced by waves and power drawn by OWEC devices is presented. Then the chapter explains the CFD implementation of the OWEC system. The general algorithm along with a specific example of OWEC systems in summer wave conditions is presented.

2.2 Basic Parameters of Ocean Waves

Ocean surface waves are random in space and time. However if the fundamental frequency is considered, waves can be considered of sinusoidal profile. The three parameters which describe wave behavior are period, height and deep water length. The wave period, T, defined as the time between two successive wave crests or troughs, wave height, H, defined as the vertical distance between the crest and trough and mean water depth, h, defined as the distance below the still water line till the sea bed.

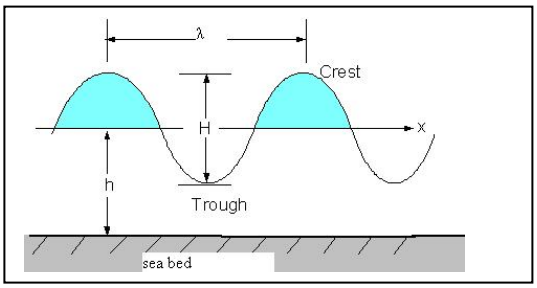

Figure 2.1 basic parameters of wave

The wave length, λ, is the horizontal distance between two successive wave crests or two successive wave troughs.

Ocean wave conditions are stochastic in nature and are often described with statistical parameters such as the significant wave height H_s and the energy period, T_e. The significant wave height is defined as the average wave height of one third of the highest waves. The wave period is defined as the reciprocal of the frequency at which the peak of power spectral density occurs [9].

2.3 Linear Wave Theory

2.3.1 Governing equations

The physical relations and properties of waves need to be carefully studied before the OWEC system design starts. The OWEC force withstanding capacity can be developed with the help of this study.

2.3.2 Properties of ocean waves

A wave whose crest moves in a direction parallel to the still water line is called a traveling or progressive wave. The phase velocity of a wave is called celerity and is given by [10],

$$C = \frac{L}{T} \tag{2.1}$$

In this section, study is limited to progressive waves because open sea waves are progressive waves.

The water can be considered incompressible, in viscid and irrotational for the purpose of study. If two-dimensional analysis is considered, much simplification is observed in derivations. We begin with Navier-Stokes equations [11, 12]

$$\frac{D\vec{u}}{Dt} = \vec{F} - \frac{\nabla p}{\rho} + v\nabla^2\vec{u} \tag{2.2}$$

$$\nabla.\vec{u} = 0 \tag{2.3}$$

The density of water ρ is assumed to be constant. The viscosity is neglected. Furthermore, it can be assumed that under the influence of wave motion, the particles move on a curved path and they do not spin about their own axis. Water particles are assumed to be stationary initially and move by normal forces exerted by waves.

If u and v are velocities of waves in x and y direction, then simplified continuity equation for two dimensions become [10],

$$\frac{\partial^2 \phi}{\partial x^2} + \frac{\partial^2 \phi}{\partial z^2} = 0 \tag{2.4}$$

Also $\frac{\partial v}{\partial x} = \frac{\partial u}{\partial y}$ [10] for x-y plane of interest is assumed to be equal. ϕ is velocity potential.

The progressive wave equation is given by [10],

$$\phi = A \cosh k(z+h) \cos(kx - \omega t) \tag{2.5}$$

A is constant and ϕ is velocity potential.

a (wave amplitude), k (wave number), c (celerity) and h (water depth) are constants.

The constants a, k, c, and h represent the properties of waves and needs to be determined.

The constant k can be determined from the periodicity of waves [10].

$$k = \frac{2\pi}{\lambda} = \frac{2\pi}{kc} \tag{2.6}$$

The wave length λ for deep water waves is given by [10]

$$\lambda = \frac{gT^2}{2pi} \tag{2.7}$$

The water is considered as deep water if water depth is at least half of wave length.

$$h \geq \frac{\lambda}{2} \qquad [8] \tag{2.8}$$

It can be observed that no water particles can cross the sea bed [10].

$$v = \left.\frac{\partial \phi}{\partial y}\right|_{y = h} \tag{2.9}$$

At water surface, it can be assumed that no particles can cross the free surface [10].

$$\frac{\partial \eta}{\partial t} = \left.\frac{\partial \phi}{\partial y}\right|_{y = 0 or \eta} \tag{2.10}$$

The pressure at the free surface (gauge) is zero. Surface tension is neglected. The dynamic equation for pressure is derived by the conservation of momentum given by [10].

$$\frac{P}{\rho} + \frac{1}{2}\rho^2 + gy + \frac{\partial \phi}{\partial t} = 0 \tag{2.11}$$

P=0, gauge pressure and ρ^2 is neglected as wave velocities are small [10].

$$\left.\frac{\partial \phi}{\partial t} = -g\eta\right|_{y = \eta} \tag{2.12}$$

$$\eta = -\frac{A}{C}\sinh kh \sin(k(x - ct)) \tag{2.13}$$

The surface boundary condition is obtained by combining equations [10].

$$\frac{\partial^2 \phi}{\partial t^2} + g\frac{\partial \phi}{\partial y} = 0|_{y=\eta=0} \tag{2.14}$$

The celerity of wave can be obtained by differentiating progressive wave equation with respect to t and y [10].

$$c = \sqrt{\frac{g}{k}\tanh kh} \tag{2.15}$$

The wave amplitude is given by [10].

$$a = -\frac{A}{c}\sinh kh \tag{2.16}$$

2.4 Mass, momentum and energy transfer by Progressive waves.

The wave particles move in circular path due to forces exerted by waves. It is interesting to understand how mass, momentum and energy is transferred by waves, as progressive waves travel long distance with little loss of energy.

The rate of mass and momentum transfer by waves is given by [10].

$$I_x = \dot{m}_x = \frac{\rho a^2 g}{2c} \tag{2.17}$$

The forces exerted by waves on floating or submerged bodies per unit width is given by [10]

$$F = \frac{1}{4}\rho g(a_i^2 + a_r^2 - a_t^2)(1 + \frac{2kh}{\sinh kh})$$

Where a_i (incident), a_r (reflected), a_t (transmitted) wave amplitude.

$$F = \frac{1}{4}\rho g(a_i^2 + a_r^2 - a_t^2) \quad (h -> \infty \text{ for deep water}) \tag{2.18}$$

The derivation of force involved calculating flux in horizontal momentum across vertical plane and the flux in absence of waves, due to hydrostatic pressure [10],

$$P_o = -\rho g h \tag{2.19}$$

The total energy is equally composed of potential and kinetic energy as given by linear wave theory [3],

$$E_p = E_k = \frac{\rho g H^2 \lambda b}{16} \quad (..b \text{ crest width}) \tag{2.20}$$

The total energy [13] of waves is given by

$$E = E_p + E_k = \frac{\rho g H^2 \lambda b}{8} \tag{2.21}$$

The potential energy is due to wave height and kinetic energy is due to motion of water particles. As the wave progresses, it transfers energy from point to point in its direction. The wave power is given by [3],

$$P = (\frac{1}{4}\rho g a^2)(gc)(b) \tag{2.22}$$

2.5 Response of devices to waves

The waves produce a periodic disturbance. When the OWEC system is deployed in the ocean, the waves exert force on the device. The force exerted by waves is periodic in nature and depends mainly on wave height, period and is given by [10],

$$F\cos\omega t\,. \tag{2.22}$$

The reaction force is produced by restoring force, damping force (friction), energy extraction (PTO damping) and the radiation force [10],

$$F\cos\omega t - D\dot{y} - Sy = m\ddot{y} \tag{2.23}$$

As can be observed from above equation, damping force is linearly proportional to velocity where as restoring force is linearly proportional to displacement.

The frequency of natural damping force due to energy extraction is given by [10]

$$\omega_0 = \sqrt{\frac{S}{m}} \tag{2.24}$$

S restoring force in N and m mass of system.

The extracted power can be calculated as [10],

$$F_i = D_e \dot{y} \tag{2.25}$$

$$P_i = (De)\dot{y}^2 \tag{2.26}$$

From extracted power, the mean power is given by [10],

$$P_{\text{rms}} = \frac{1}{2} D_e \dot{y}^2 = \frac{1}{2} D_e c^2 \omega^2 \tag{2.27}$$

c added mass coefficient, De is damping coefficient.

2.6 CFD implementation

2.6.1 Numerical grid

The solution domain is divided into four blocks. A rectangular grid is used for all blocks. Buoy is fitted in the middle block. Middle block resolution is quite high to maintain the accuracy of solution. This block is repeatedly moved after each time step to maintain the structural integrity. The block is fitted to the buoy which is moved up and down with the help of API. The blocks adjacent to the buoy block forms a stationary grid and is not regenerated for each time step. The block close to the beach is structured unevenly to provide a damping effect to the waves. The grid continues decreasing towards the beach end. Please refer to fig. 2.2.

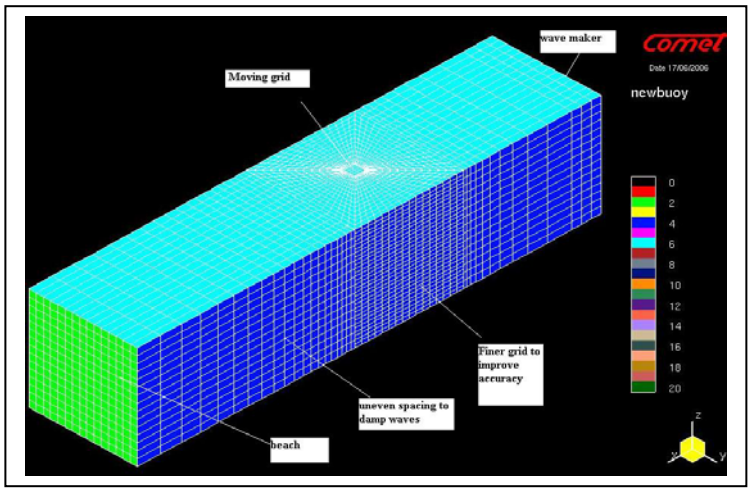

Figure 2.2 Grid generation CFD

The wave maker is formed by a rectangular grid and forms part of the moving grid at each time step. The piston type wave maker is formed by the boundary wall and moved at sinusoidal profile.

2.6.2 Boundary conditions

Boundary conditions are applied to the solution domain. The no-slip boundary condition is applied to the wave maker. The velocity of the wave maker is imposed on wave particles adjacent to the wave maker. The buoy surface is also given a no-slip boundary condition. Therefore the velocity of water particles adjacent to the buoy is the same as the buoy velocity [14]

$$U_i|_{fluid} = V_i|_{fluid} \tag{2.28}$$

For the outer boundary condition, a preceding block provides a numerical damping with increasing cell volumes at the beach end. If the outer boundary condition is not sufficient for bigger wave heights, artificial damping scheme based may be employed.

The wave maker stroke is given by [15],

$$s = H/2 * \sin \omega t \tag{2.29}$$

The stroke is adjusted so as to get the required height of the wave. The height of wave can be analytically checked using a piston wave maker surface elevation, given by [15].

$$\phi = \frac{4s \tanh kh \sinh kh}{\omega(2kh + \sin 2kh)} \cosh k(z+h) \cos(kx - \omega t) \tag{2.30}$$

$$\eta(x,t) = -\left.\frac{\partial \phi}{\partial t}\right|_{z=0} = \frac{4s \sinh^2 kh}{2kh + \sinh 2kh} \sin(kx - \omega t) \tag{2.31}$$

Where s is stroke and k is wave number.

2.6.3 Force displacement coupling.

The buoy displacement is determined from the dynamic solution of the buoy and fluid (composite air-water) interaction. The fine mesh is fitted to buoy and regenerated with each time step. The net instantaneous forces acting on the buoy can be determined from comet solver. The obtained forces are used to find velocity, displacement of buoy with the help of mass and time step. Refer to fig.

2.3. The average values are used in the calculation. Comet API (application programmer's interface) is used to determine new position of buoy after considering PTO damping coefficient.

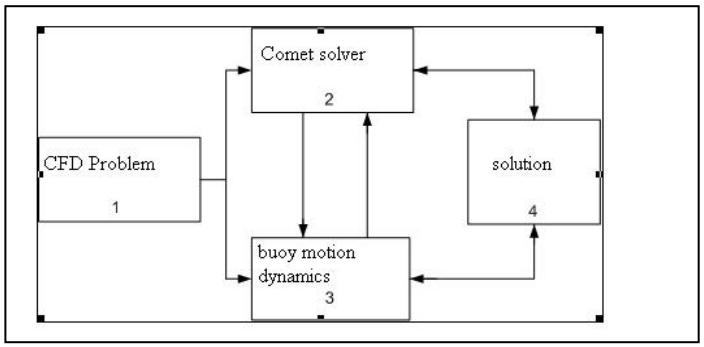

Figure 2.3 Force displacement coupling

The buoy dynamics is governed by Newton's second law of motion [14]

$$m\ddot{U} = F_{wave} + F_{wt} + F_{pto} \tag{2.32}$$

F_{wave} is net force calculated using comet solver; F_{wt} is weight of buoy acting in negative z direction. F_{pto} is power take off force; m is mass of buoy and $\ddot{U}$ is acceleration of buoy [14]

$$F_{pto} = b_d \dot{U} \tag{2.33}$$

$$P_{pto} = b_d \cdot \dot{U} \cdot \dot{U} \tag{2.34}$$

The PTO force acting on the buoy is calculated as the product of PTO damping coefficient b and the heave velocity of buoy. The pneumatic power across the

damper is given by the product of PTO force and the heave velocity. The updated values of velocity and displacement are given by [14]

$$\dot{U}_{n+1} = \dot{U}_n + \frac{\Delta t}{m} F_{av} \tag{2.35}$$

$$U_{n+1} = U_n + \Delta t \cdot \dot{U}_{av} \tag{2.36}$$

Implicit Backward Euler's time integration scheme is used to obtain the average values force F_{av} and velocity $\dot{U}_{av}$ [14]

$$F_{av} = \frac{1}{2}\left(F_n + F_{n-1}\right) \tag{2.37}$$

$$\dot{U}_{av} = \frac{1}{2}\left(U_n + U_{n-1}\right) \tag{2.38}$$

The general algorithm for CFD solver is given by

1) Grid generation for each block
2) Impose initial conditions
3) Impose boundary conditions
4) Solve Navier-Stokes equation using comet solver
5) Coupling algorithm is executed for wave force-buoy displacement.
6) Regeneration of moving grid
7) Repeat 4-6 with each time step.

The numerical tank is filled with air and the water is considered as add on species. This makes air-water as composite fluid. The scalar indicator, volume of fraction c, is used to distinguish cells filled with air and water. Value of one is

assigned to cells filled with water and value of zero is assigned to cells filled with air [14]

$$\frac{d}{dt}\int_V c \cdot dV + \int_S c \cdot (v - v_s) \cdot dS = 0 \tag{2.39}$$

The transport equation (2.39) is solved to obtain the current value of velocity of buoy cell. In the above equation v_s is characteristic velocity of fluid, V is the cell volume, S cell face area, v velocity of buoy cell. Front capturing method with HRIC (High resolution interface capturing) scheme is used to obtain the deformation of free surface. HRIC scheme is combination of upwind and downwind differentiating schemes, provides interface between two fluids and is based on convective transport of volume of fraction c.

2.7 Single buoy CFD simulation analysis

The instantaneous power captured by the buoy depends on PTO damping and velocity of the heaving buoy (2.27). The power is calculated for two wave climates, summer and winter. For 0.25 setting of PTO damping, the instantaneous power for summer can be observed in fig. 2.4. For summer conditions, the total power from waves is calculated using [15]

$$P = \frac{\rho g H^2 T}{32 pi} \qquad \text{kW/m} \tag{2.40}$$

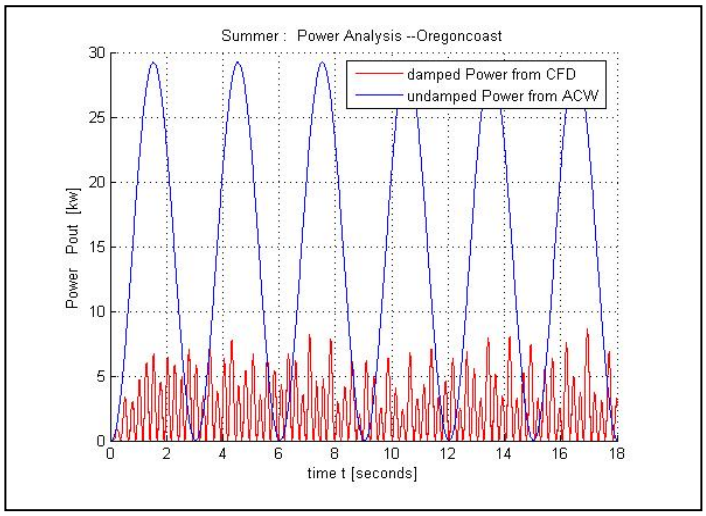

Figure 2.4 Wave power captured by OWEC system

The buoy of 4.5m diameter produces peak power of 6 kW as can be observed in fig. 2.4. The displacement, velocity and forces acting on the 100th scale buoy are plotted in figs. 2.3, 2.4, and 2.5 respectively.

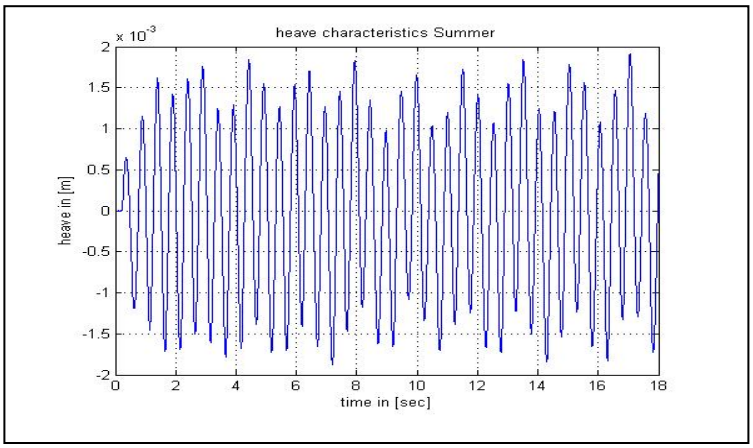

Figure 2.5 Heave displacement in m

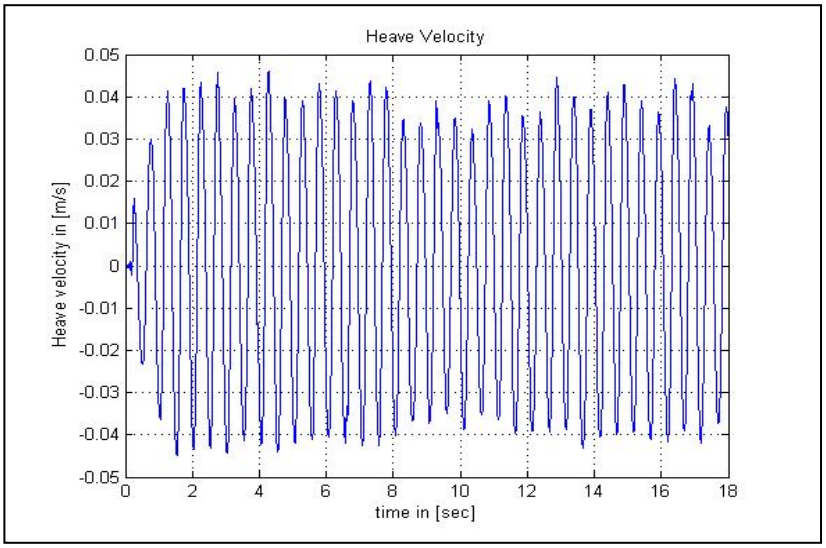

Figure 2.6 Heave velocity in [m/s]

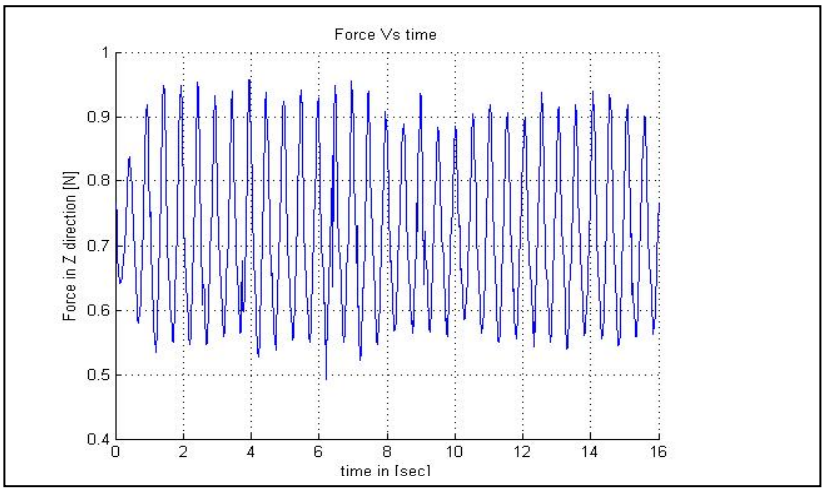

Figure 2.7 Force in z-direction [N]

The plots were showing a period of 0.25 sec which is quite high as compared to wave setting of 0.6 sec. This problem occurs due to non-synchronization of force-displacement coupling to buoy using application programmable interface (API). So the obtained data is sampled and passed through the low pass filter to remove unwanted high frequency noise.

The profile of wave forces is sinusoidal as the numerical wave tank produces monochromatic waves. The buoy heave motion is lightly damped by PTO damping as show in fig. 2.8. The heave shows uneven peaks at low frequencies indicating the presence of harmonics. Refer to fig. 2.5. The forces in x and y direction are not plotted as the heave motion in the z-direction is the focus of the study. However, for other motions like sway or pitch, the forces in these directions must also be considered.

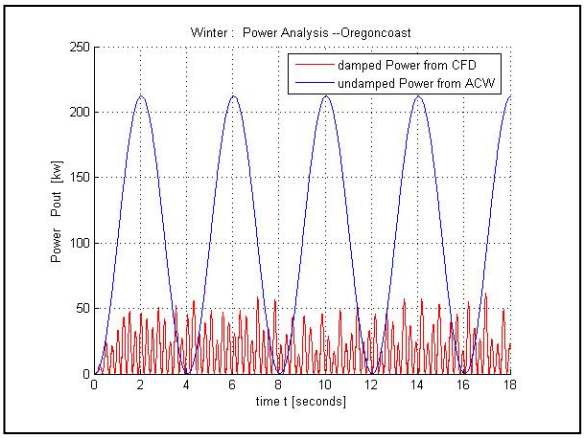

Figure 2.8 power captured in winter

The power profile for winter is plotted in fig. 2.8. As can be observed from the plot, the wave power is 6-7 times the wave power observed in summer.

The velocity vectors showed up and down movement, similar to the buoy up and down movement. Please refer to fig. 2.9.

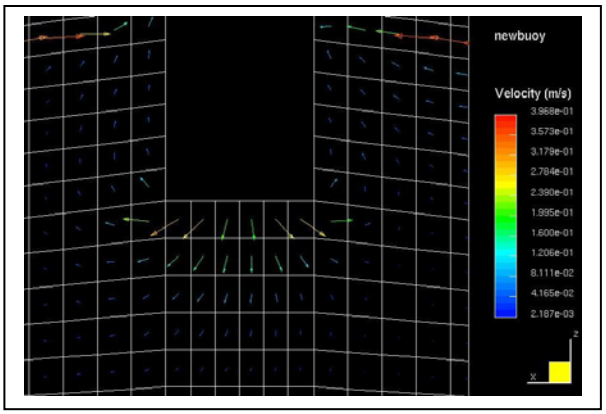

Figure 2.9 Downward velocity vector

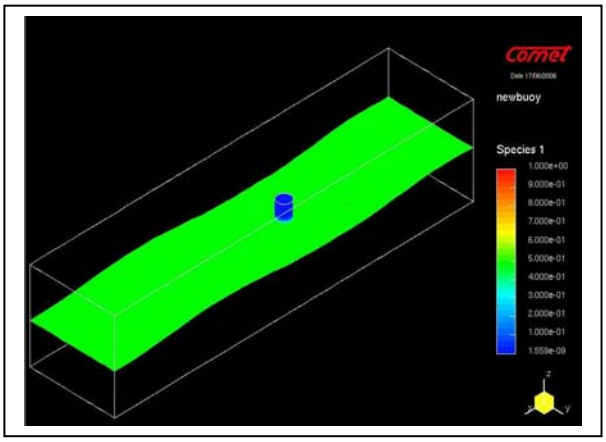

Figure 2.10 Single buoy heaving in waves

The efficiency of electrical machines and mechanical efficiency of converting wave force into thrust is not taken into consideration in the wave flume results. These parameters can be calculated and plugged back into the CFD model to obtain the accurate power estimate. Also it is relatively easy to change the buoy dimensions and check the results once results from flume match the CFD results.

2.8 Summary

A numerical method to simulate fluid-solid interaction is demonstrated. The governing equations are presented. COMET software is used to implement CFD code. The complex grid is generated for moving parts in the system like buoy block. The buoy is made up of cylindrical shape. The coupled force-displacement algorithm is applied. The results obtained are plotted to understand the net instantaneous forces acting on the buoy. The heave velocity of the buoy is plotted. The power obtained under damped conditions is plotted.

The code makes assumptions for dynamic pressure and surface tension. For accuracy of code, the results must be verified experimentally. Moreover the complex buoy shapes are difficult to implement as the software is quite resource intensive. Alternate CFD software must be investigated to model internal details of OWEC systems. The only advantage with CFD solution is once one result is verified experimentally, the buoy dimensions can be varied to obtain optimum dimensions and the capacity factor of the system can be studied.

CHAPTER 3. WAVE FLUME DESIGN

3.1 Introduction

The ocean wave experiments are usually carried out on a scaled model to better understand the fluid-solid interaction. In the present study a 100^{th} scaled model of prototype design is considered and a wave flume is designed using the scaled dimensions. First a wave flume design is presented. Then the effect of scaling factor on various dimensional quantities of interest is presented. Finally the experimental set up for the wave flume is very briefly discussed.

3.2 Wave Flume Design

The wave flume helps to understand ocean wave behavior and investigate fluid-solid interaction under controlled conditions. In a general wave flume, the waves are excited at one end using a wave maker device. The wave maker device may be of plunger, piston, and flap type. A detailed discussion on types of wave maker is available in many excellent books. [15,16].

In this design a piston type wave maker is considered due to its simplicity and robustness. The excited waves travel along the length of wave flume. The ocean buoy which is cylindrical in shape heaves in Ocean waves. At the other end of the flume, the energy in ocean waves is absorbed with the help of an artificial beach. The inclination of beach to waves must be adjusted to avoid reflection.

Another method is to identify reflection of waves and reduce the stroke of wave maker to avoid reflection. Such a method is useful in very small flumes.

The significant wave height is considered in the design process. For the Oregon coast the significant wave height and period are tabulated in the following table. Also the scaled model parameters are listed in the table.

	Wave Condition		Scaled Wave conditions(1/100th Scale)		
	Winter	Summer	Winter	Summer	Units
Hs	3.5	1.5	0.35	0.15	(m)
Ts	8	6	0.8	0.6	(sec)
S			0.31	0.01	(m)
λ	99.84	56.26	0.99	0.56	(m)
$\frac{\lambda}{2\pi}$	15.8	8.95	0.15	0.09	(m)

Table 3.1: Wave conditions

Since the wave flume is designed for the Oregon coast, the range of period useful for analysis is 0.5-2 sec and the range of stroke useful is 0.5-8 cm approximately. The stoke values can be adjusted practically to achieve the required wave height.

The buoy in the wave flume acts as a point absorber. The power absorbing periphery is as shown in fig. 3.1.

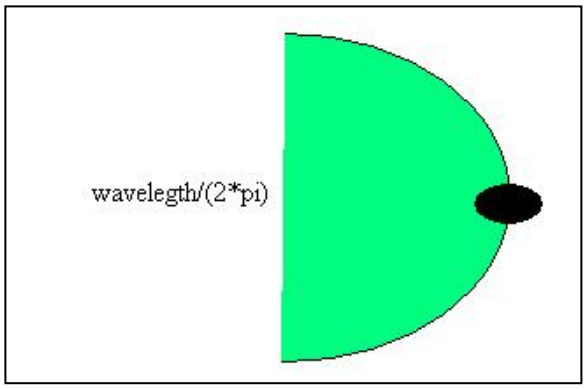

Figure 3.1 wave power absorbing periphery

From table 3.1 above, the maximum power absorbing periphery is for winter conditions, so a total of 4 times the periphery makes the width of the tank. If two buoys are tested side by side, it can be observed that their power absorbing peripheries do not overlap. This dimension ensures that there is no reflection from side walls. Refer to fig. 3.2. The deep water for engineering purpose is defined as [3]

$$h \geq \frac{\lambda}{2\pi} \tag{3.1}$$

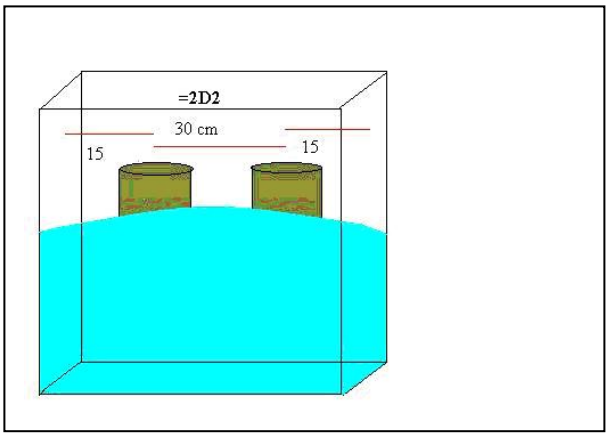

Figure 3. 2 Side by side distance of buoys.

The depth of the tank is selected as 1.2m which is greater than the required depth for winter and summer deep water conditions. Moreover the depth of water can be varied by raising or lowering water in the tank. The length of tank can selected at least 3.5 times the wavelength of the waves under consideration for array of buoys. The actual length is 9m which is more than the required length to accommodate space for wave-maker and artificial beach.

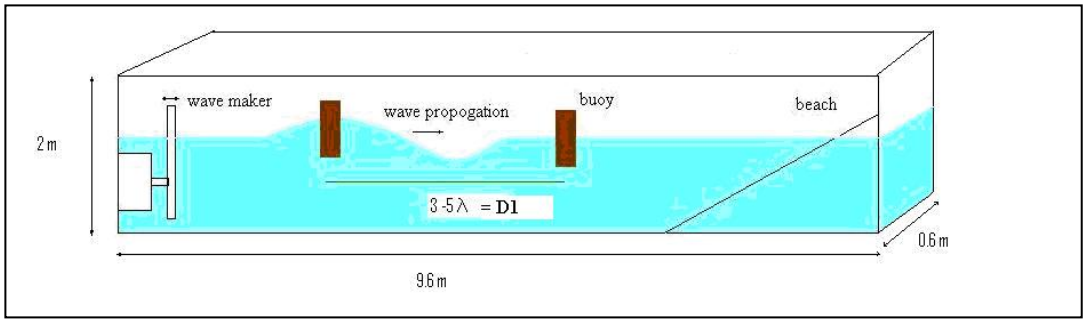

Figure 3. 3 Dimensions of wave flume.

The final dimensions of the tank are as shown in fig. 3.3

It is theoretically and experimentally proved by Budal [10, 17], the interaction factor q defined as the ratio of maximum power generated by the buoy with interaction to maximum power generated by a single buoy without interaction. If the ratio is set to 1, then the power generated by a single buoy would be as if generated by a single buoy without interference. In present case, the ratio of buoy spacing to wavelength ratio is of the order of 3-5 times. Please refer to fig. 3.3 and following table:

Scaling factor 100		
	Parameter	Value
d	diameter of buoy	4.5 cm
D1	Length wise distance	307 cm
D2	Width wise distance	15 cm

Table 3.2 : Scaling factor

For testing operation of arrays of buoys, the interference free distance is ensured. So long as the horizontal distance between two buoys in greater than $\lambda / 2\pi$ and the vertical distance between two buoys is greater than λ there would be no interference. Please refer to fig. 3.4.

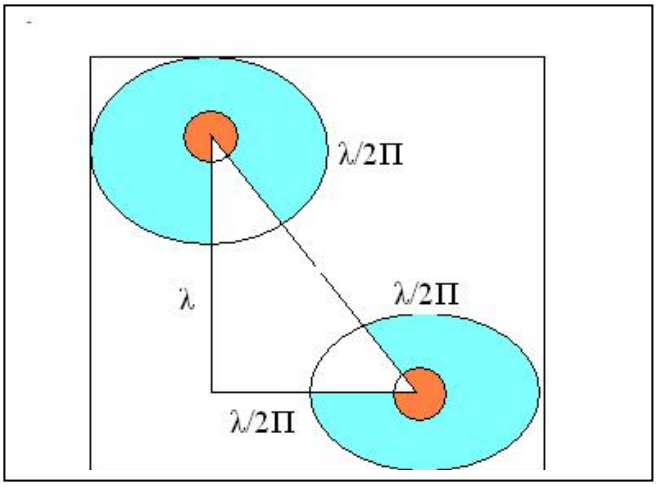

Figure 3.4 Buoy spacing

3.3 Scaling factors

The scaling factors ensure that dimensions, kinematics and dynamic behavior are unaltered in model and prototype. The inertial forces and gravity forces are important parameters in free surface flow. The scaling is based on Froude Law. The Froude number Fr is defined as the square root of ratio between inertial force to gravity force and is given as the following [18],

$$Fr \geq \frac{U}{\sqrt{gL}} \tag{3.2}$$

The Froude number for both model and prototype is kept the same. Observe in the following table acceleration is same for model and prototype. Also the density is same for model and prototype.

Parameter	Scaling factor α
Wave height (m)	$H_S = H_F / \alpha$
Wave velocity (m/s)	$v_S = v_F / \sqrt{\alpha}$
Wave acceleration (m/s s)	$a_S = a_F$
Wave period (sec)	$T_S = T_F / \sqrt{\alpha}$
Power (w)	$P_F = P_S \sqrt{\alpha^7}$

Table 3.3 Scaling of other dimensions [18]

The length and height of wave flume is selected such that the natural frequency of oscillation of flume in not integral multiple of the wave frequencies under study. The natural frequency of oscillation of the flume is given by [15]

$$f_{Flume} = \frac{n\sqrt{gh}}{2L} \tag{3.3}$$

In the above equation if n is varied from 1, 2, 3… the natural frequency of oscillation of flume is given by 0.2307, 0.46, 0.69… Hz

The frequencies of waves under study are 0.125, 0.167. The two frequencies are not integral multiples, so there would no effect of resonance.

3.4 Experimental Setup

The overall dimensions of flume are 9.6m long, 0.6 m wide and 2 m deep. The piston type wave maker is selected for operation. Active wave absorption ® may be used along with piston wave maker to absorb reflected waves. The readers are requested to follow the reference [19] for further information. The wave maker and the artificial beach will occupy 1m on each side of the tank. Further 1m is required to set up a false bottom at the other end of the flume. The remaining 6.6m flume is available for testing of OWEC systems. The bottom and side walls can be made from glass. This helps in velocity measurement. The ruble mounds structures can be prepared to create artificial beach. The characteristics of gravel such as porosity, density can be studied before implementation. Also water can be re-circulated by providing a hole between the horizontal surface and the inclined surface. The whole structure can be appropriately supported by steel beams.

3.4.1 Instrumentation

Free surface gauges can be used to measure the elevation of waves. A separate set of gauge can be used for incident and reflected wave measurement. The pressure gauges can be mounted at the bottom structure. A portion of glass structure can be supported by steel frame for this purpose. The wave velocity can be measured with the help of Acoustic Doppler Velocimeter (ADV). Further a

Llaser Doppler Velocimeter (LDV) can be used to measure the velocity of heaving buoy. Refer to fig. 3.5, 3.6 for general information.

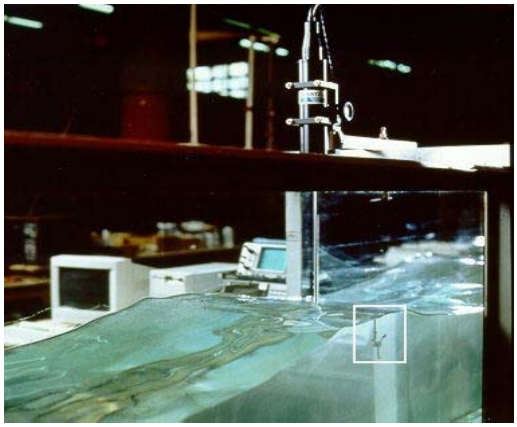

http://www.sontek.com/apps/flume/adv-swf/adv-swf.htm

Figure 3.5 ADV for measurement of wave velocity

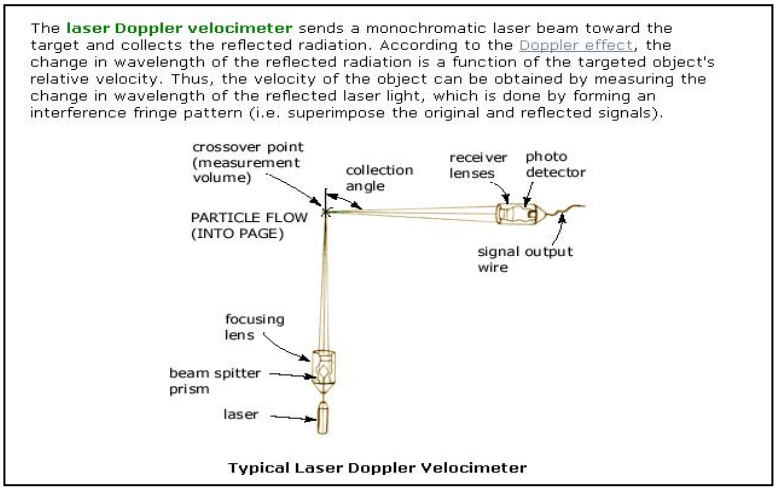

Figure 3.6 Laser Doppler Velocimeter

4. DIRECT DRIVEN PMLG DESIGN USING FEM

The linear generator offers robust energy conversion mechanism for OWEC system. Due to decrease in price of NdFeB magnets, new research in linear generators is possible. NdFeB magnets produce high magnetic flux density thereby helping to reduce the system weight. Also linear generators couple heave motion of waves to generate power with a simple power take-off mechanism. This reduces the need of maintenance and makes the generator suitable for Ocean Wave applications [20].

In this section, first the design of a linear generator is discussed. Primarily dimensioning of the system, thrust calculations, stator slot mmf calculations and emf calculations are discussed. In appendix A, a MATLAB script is provided to understand equations used to find results [8]. Then parametric analysis is carried out by varying magnet height, slot depth, slot opening and number of conductors. The dependence of output power, emf, and current on these parameters is studied with the help of graphs. The parameters are selected based on high efficiency design of the generator.

These parameters are then plugged in Maxwell 2D FEM modeling software. The air gap flux density and the thrust are calculated and compared against the analytical calculations. It is observed that peak values assumed in the design are close enough as obtained from FEM. The PMLG is designed to deploy in the wave flume. So the model dimensions are selected as 100^{th} scaled dimensions.

4.1 Introduction

Linear generators utilize short progressive linear motion to produce electrical power. The linear motion between the stationary translator and the moving stator (core-coil assembly) is utilized to a produce change in flux and thereby generate emf. Due to its compactness, high efficiency, and ability to produce high thrust, it finds application in OWEC systems.

The tubular (PM) design is forms the part of study because of its advantages over flat design. The tubular design has less leakage flux and the design parameters can best be optimized to achieve higher (emf) and efficiency (η) [21].

In spite of the above mentioned advantages, tubular (PM) design has to overcome higher cogging force. The cogging force is produced due to an abrupt change in flux density caused by different geometric structure of stator and translator. Due to the pulsating nature of cogging forces, vibrations and noise are produced.

The proposed design optimizes the dimensions of PMLG and finds the thrust. The design is optimized for best efficiency. Also the machine is able to create high thrust to match the slow rising high thrust nature of ocean waves.

4.2 Overview of PMLG structure

A stationary vertical spar is anchored to the sea floor. The magnets are mounted on the spar as shown in fig. 4.1. This part is also called an active spar or translator. The armature consists of core-coil assembly inside the active float (buoy). The armature and translator are isolated by an air gap. The buoy heaves in ocean waves, which moves the armature relative to a stationary translator. This relative motion causes a change of flux, there by generating emf in the armature

coils. The above construction of magnets inside and coils outside is selected as it is expected to minimize the cost of the system.

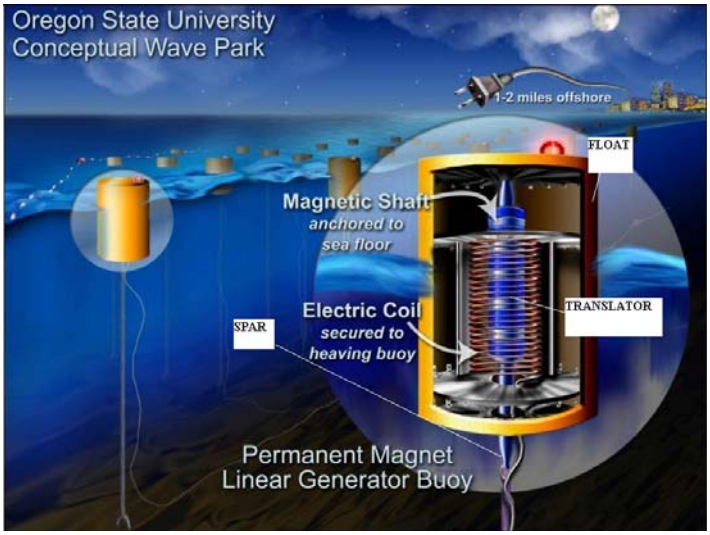

Courtesy Oregon State University, Electrical Engineering Dept

Figure 4.1 Overall picture of buoy

4.3 Design Calculations

The design starts by considering a required outer diameter of armature as 0.047m. The diameter of the spar is considered 0.018m as it makes the spar more robust. The stroke length for winter waves is considered from significant wave height as 0.035m for 100^{th} scaled model. The peak linear speed of generator is obtained from significant period (8 sec) of waves for winter season. These values are based on Oregon Coast wave conditions.

4.3.1 Magnetic circuit design

Four pairs of high density NdFeB35 magnets are used. The direction of magnetization is normal to the axis of symmetry (radial). An attempt has been made to check if it gives high efficiency. The slot pitch and pole pitch are kept unequal as can be observed in fig. 4.1. The dimensions are set after checking the effect on efficiency. The non-magnetic spacers are placed between magnets to avoid short circuit. A suitable high strength and low weight material needs to be used, however Delran may be used as non-magnetic spacer.

The spar made up of high quality steel material provides the return path for flux as can be seen in fig. 4.2. The air gap between the armature and translator is kept as 1mm to simply construction. However in large machines, the air gap length must be optimized.

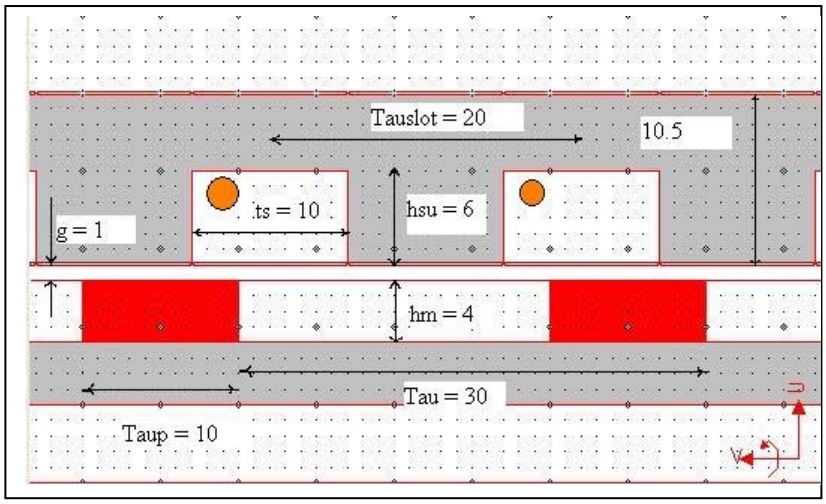

Figure 4.2 PMLG dimensions in mm

The value of air gap flux density is set as 0.6 T [8] and spar flux density is set as 1.02 T [8]. The value is selected so as to avoid magnetic flux saturation in spar.

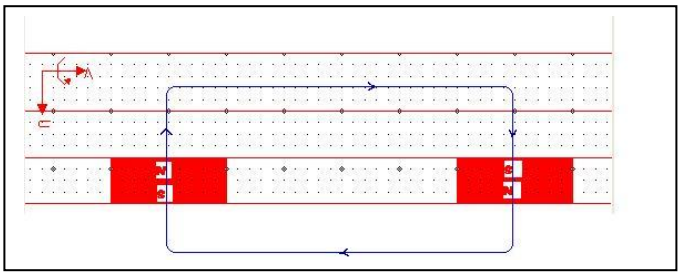

Figure 4.3 Flux path in PMLG

The slot opening is set as two third of slot pitch. This parameter is selected so as to achieve the required voltage and current levels. The air gap flux density 0.6T can be used to calculate magnet ring height and it is 4mm. After obtaining magnet ring height and Carter coefficient (due to the fringing effect, magnetic flux in the air gap of electrical machines is reduced. This leads to enlarged effective air gap length. The Carter coefficient is applied to compensate the slot effects), the equivalent magnetic air gap can be calculated and it is 7mm. This is a little higher value. However it is retained in the design as it keeps the armature reaction low. Values of magnetic ring height and air gap length can be used to calculate the inner diameter of the armature and it is calculated as 30mm. This makes the outer dimensions of float as 0.047m and inner diameter as 0.030m. The flux density in the outer core of the armature is assumed to 1.37 [8] T. This is to avoid saturation. In slot depth calculations, it is necessary to consider inner and outer diameters of armature. The slot depth is calculated as 6 mm. The flux density in the spar needs a check as it may get saturated or excessive forces might get developed in it. It is

calculated and found to be 0.8519 T. If it is excessive or very high then iron shunting rings might be required to be embedded in between the two magnets.

4.3.2 Thrust and stator slot mmf calculations

The high thrust developing capacity of PMLG is critical as the application is in low velocity Ocean Waves. The various forces acting on PMLG can be resolved to find peak thrust. The product of no of conductors and current must be kept high to develop high thrust for continuous operation. Keeping current high increases losses and thereby lowers efficiency. So a balance is observed and the value of peak thrust calculated is 28.35 N.

4.3.3 Losses in magnetic circuit.

Losses in the magnetic circuit are made up of two components, the losses are in core and in pole tips. The flux density in pole tips rise as the tip passes pole, remain constant and then decrease as the tip leaves the pole. Please refer to fig. 4.4. The losses increase as the frequency of operation and the flux density in the tooth increase. The frequency of operation is low due to slow rising ocean waves and the flux density is kept low to avoid saturation (1.37 T). The above statement is also applicable to core loss. The only difference between these two types of losses is that the pole tip loss rises very sharply and decreases very sharply. However the core loss is slow varying with frequency. The total core loss calculated for design is 1.9mW.

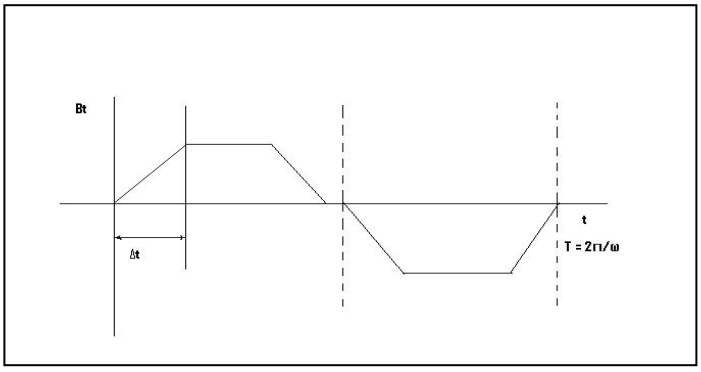

Figure 4.4 flux density changes in pole tip

4.3.4 Electrical circuit design

The selection of current density is a critical factor in electrical circuit design. The maximum current density is given by [8],

$$(J_{co})_{\max} = \frac{n_c * \mathrm{I_m}}{h_{su} * t_s * K_{fill}} \qquad (4.1)$$

The maximum current density for design is restricted to 0.2 A/mm$^{2.}$ However the maximum current density that can be reached with out excessive temperature rise (115^{o}C) is 3.5 A/mm^2 [21]. The low current density setting lowers the current in circuit there by lowering copper losses and increasing efficiency of system. However if high power output or high thrust development is necessary, then the current density must be increased. The fill factor of the coil is assumed to

be 0.75 (The coils occupy 75% of available slot area). The full load copper losses calculated are 38 mW.

The value of resistance and inductance for 50 coil turns is calculated as 4.75 ohm and 12.7 mH. The values are based on current density selection and the product of $n_c * I_m$. The value of current and resistance are inversely proportional, so the product essentially remains constant. The time constant for the circuit is 2.7 ms. The changes in current and voltage are quite fast. The wire size calculated for the coil is AWG 26-27 or 0.75 mm.

4.3.5 Field and force calculation

If A is magnetic potential [21], the equation for the PMLG is given as,

$$\Delta \times \left[v(\Delta \times A) \right] = \Delta \times (v\mu_{0M}) + J_o^{[11]} \tag{4.2}$$

where v is magnetic potential, μ_0 permeability of free space, M is the magnetization vector, J_o is the exciting current in the coil.

The cogging force is given by [21]

$$f_n = \frac{1}{2\mu_0}(B_n{}^2 - B_t{}^2) \tag{4.3}$$

$$f_t = \frac{1}{\mu_0}(B_n \; B_t \;) \tag{4.4}$$

Cogging force can be estimated using above equations and it is roughly found out to be 15 N/cm^2

4.3.6 Emf calculation

The emf across the armature coils is calculated using Faradays law of electromagnetic induction and given by [21],

$$Emf = -N\left(\frac{d\phi}{dz}\right)\left(\frac{dz}{dt}\right) \qquad (4.5)$$

refer to the ACRONYMS section for the definition of above terms.

4.4 Parametric dimensions study for optimization of Design

The effect of various design parameters on current, output voltage, efficiency and output power can be studied to optimize the design. The parameters are selected based on the desired output.

4.4.1 PM height h_m selection

Efficiency and emf is found to be linearly increasing with increase in magnet height whereas current is found to be decreasing. The value of 5 mm is selected as it gives 96% efficiency, 5 V as emf, 0.22 A as current.

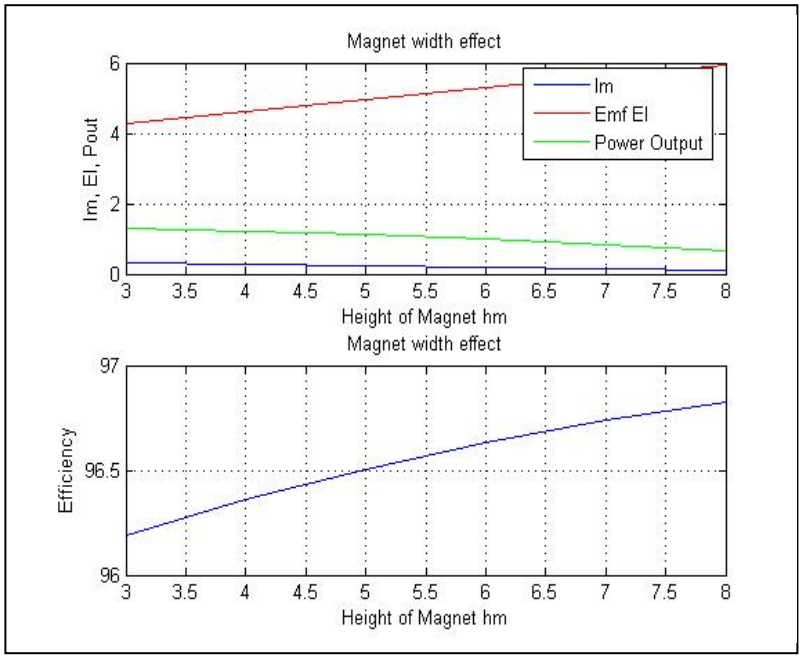

Figure 4.5 Effect of magnet width on current, voltage, efficiency

4.4.2 Slot depth h_{su} and Slot opening t_s selection.

The load current I_m & efficiency are found to be linearly increasing with slot depth. For slot depth of 6mm, the current is found to be 0.22 A and efficiency as 96 % as shown in fig. 4.6.

For even slot dimensions, efficiency, emf, current and output power linearly increase, whereas for odd slot dimensions the quantities remain constant except that the current is found to decrease. For no load parameters, the slot opening is found to be 10 mm fig. 4.7

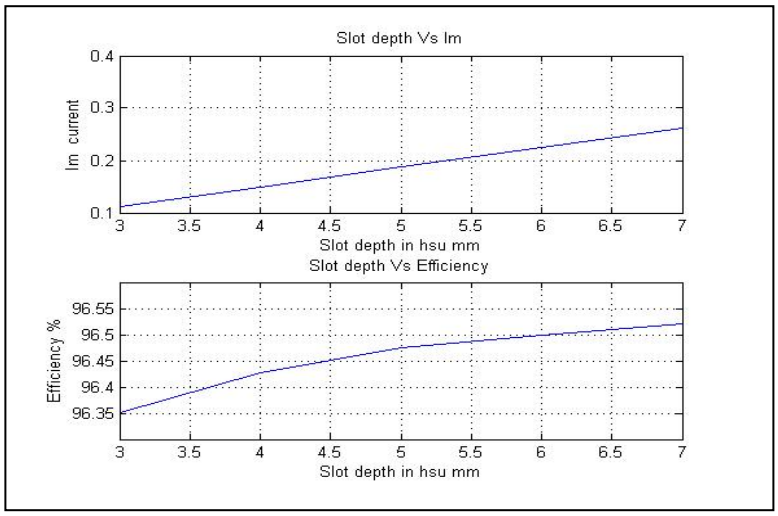

Figure 4.6 effect of slot depth on current, efficiency

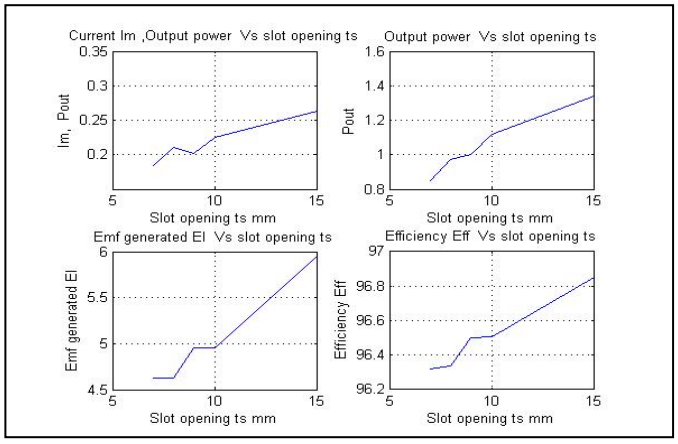

Figure 4.7 Number of conductors N_c selection

The increase in number of conductors reduces current whereas emf linearly increases. As the current increases, the efficiency reduces due to an increase in copper loss. For the present design N_c is selected as 50 as shown in fig. 4.8.

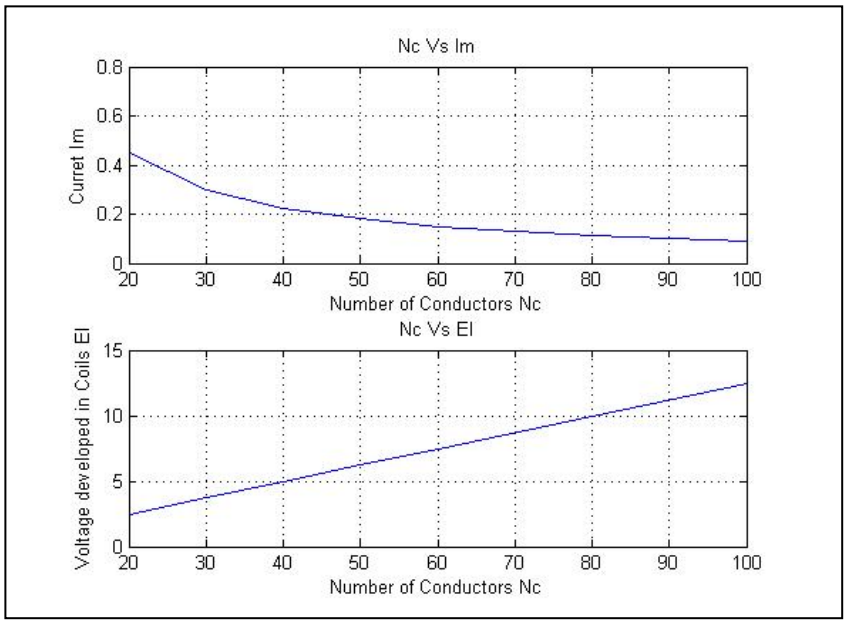

Figure 4.8 Effect of no of conductors on current, emf generated

The generator is loaded using a resistive load. The electrical circuit can be found in fig. 4.9. The output power and current is found to decrease with an increase in load resistance, whereas the voltage and efficiency is found to increase with load. The voltage regulation is defined as the difference of no load voltage and full load voltage with respect to no load voltage. It is found to be 5.65%.

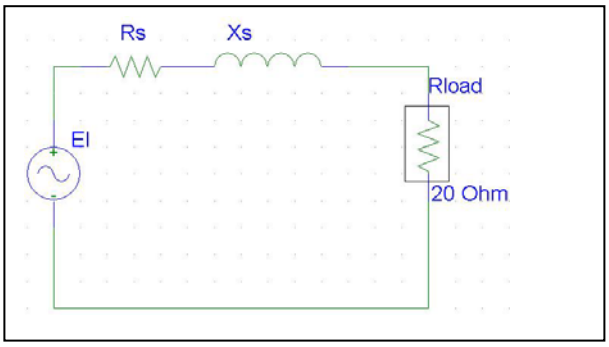

Figure 4.9 Electrical circuit of PMLG loading

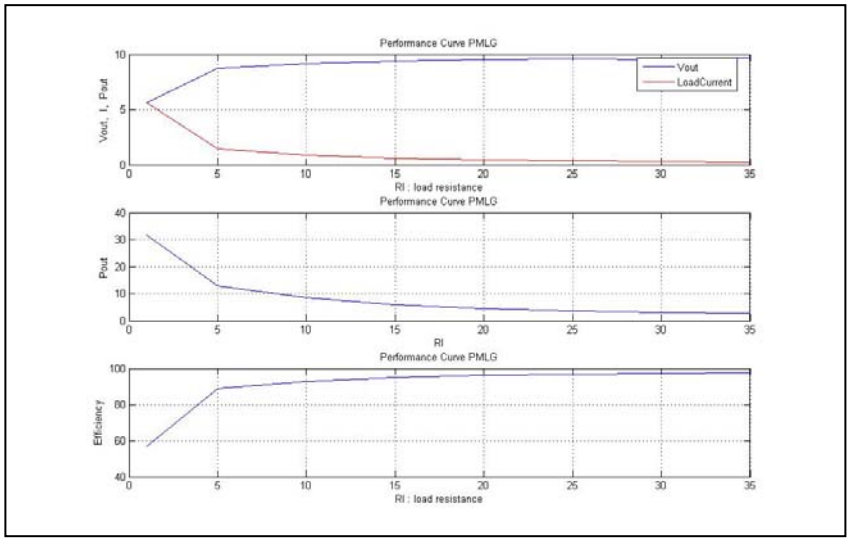

Figure 4.10 Performance curves PMLG

4.5 Verification of Design using FEM

The dimensions obtained after optimization are used in Maxwell 2D FEM software. The results from finite element modeling provided checks against the estimated values of thrust, air gap flux density and thereby emf generated in the machine.

The peak value of flux density assumed in the design (0.6) is found to be a little lower than the results of FEM calculations (0.8). Please refer to fig 4.11. The relative permittivity of core is set to 200 AT/wb which is based on practical values found in core materials [8]. The analytical values are pessimistic, however close enough to shown in FEM.

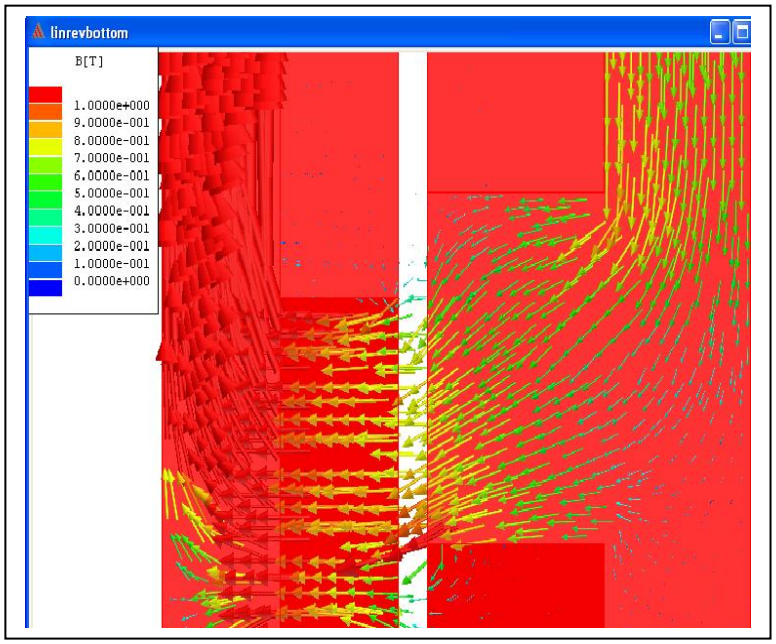

Figure 4.11 Magnetic flux density in air gap

The magnet co-energy (fig 4.12) is found to increase sharply as it reaches the pole tip and remains constant over the length of magnet and then found to decrease as the pole tip goes away from the magnet. This behavior is quite similar to the flux density variation in pole tips.

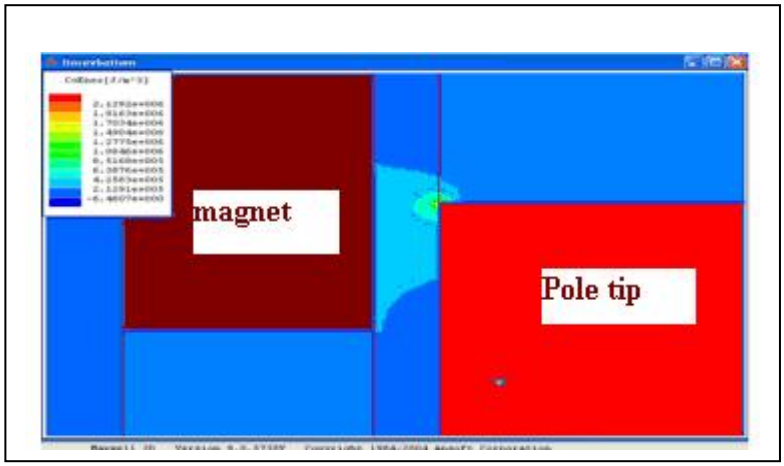

Figure 4.12 Magnet co-energy in the air gap

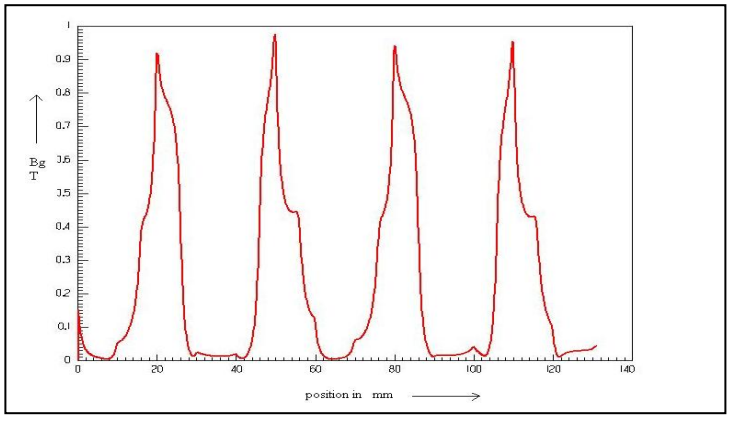

Figure 4.13 Flux density variations in air gap

The ocean wave profile for winter is considered in the design. Please refer to fig. 4.14. The efficiency of wave force conversion into the linear motion of the float is assumed to be 20%. Further the efficiency of the PMLG as calculated earlier is kept as 90%. After inserting the flux density profile obtained from FEM, the nature of pulsating emf generated can be observed in fig. 4.14. It can be observed that the emf envelop is sinusoidal due to the linear force exerted by sinusoidal wave force. However pulsations in flux density due to variation in co-energy of magnet, makes emf pulsating. The peak value of emf is found to be a little lower due to the assumption of lower air-gap flux Density.

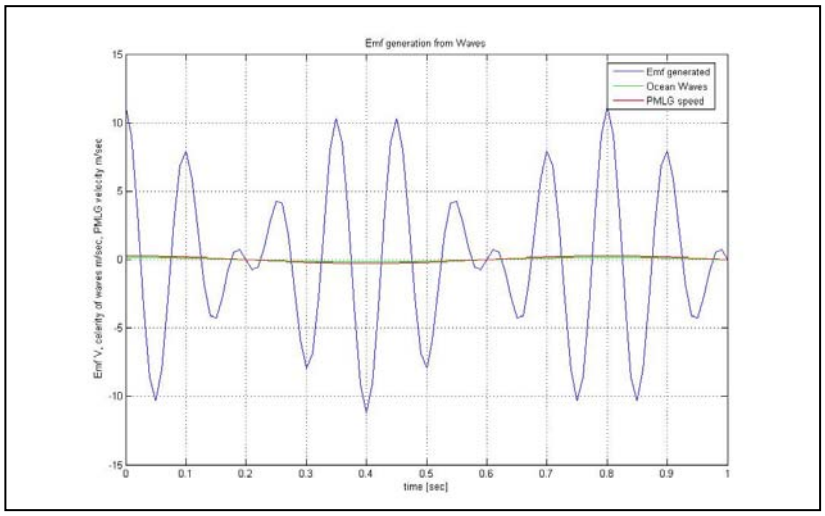

Fig 4.14 Emf generated in PMLG

4.5.1 Peak Thrust

The peak thrust profile generated by the FEM program is plotted as shown in fig 4.15. Also the peak value of thrust for the winter profile is calculated using [10].

$$F_{pk} = \frac{1}{4} * \rho * g * (A^2 - A_t{}^2) * d \tag{4.6}$$

A is the incident wave amplitude. The value of A_t (the amplitude of transmitted wave after collision with float) is neglected. As can be observed in fig. 4.15, the peak value generated by FEM analysis is higher than that provided by waves. The machine has higher capacity than peak thrust produced by waves. The analytically calculated value of peak thrust is lower than FEM, because of the assumption of lower air gap flux density.

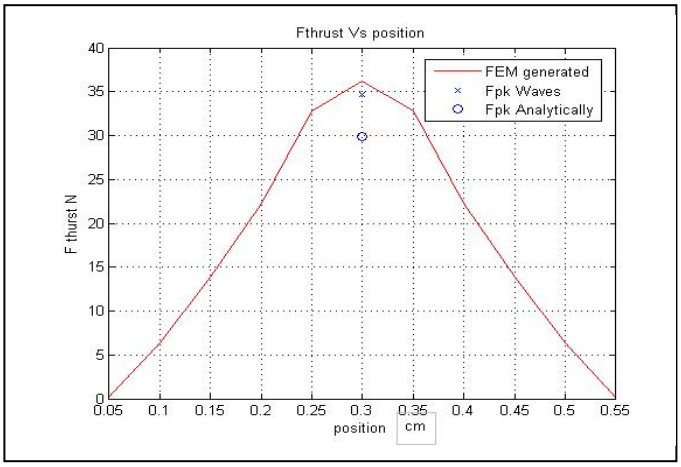

Figure 4.15 Peak trust in N/ cm^2

4.6 Conclusion

In this section a thorough analysis of PMLG is discussed. The parameters are optimized for the best efficiency design. The peak thrust is analytically calculated. The generator performance curves are drawn. As can be observed for a rated load of 20 ohms, the generator produces 10 V output voltage, and a current of 0.22 A and the efficiency of machine is greater than 90%.

The designed is verified using FEM modeling. The air gap flux density variation is obtained from FEM. The check on analytical calculations is made by comparing the peak value of air gap flux density. It is observed that the analytical calculations are a little low due to practical values set in the analytical design.

The peak thrust value calculated from FEM is a little higher than the analytical value. The cogging force is not optimized and forms the part of future study. Also, new FEM software which can perform dynamic modeling needs to be investigated.

5. BUOY DESIGN AND WAVE SPECTRUM

5.1 Introduction

When a cylindrical buoy system is deployed in ocean waves it heaves with ocean waves. The buoy system consists of a float, spar and damper ring. The float heaves with ocean waves. The float moves about the spar which is long and damped by slack mooring to the sea bed. The bearing between the spar and float should be made to minimize friction.

In this section, the friction between spar and buoy is neglected. The coupled motion is separated into two individual functions. The reason for this separation is that it makes the analysis simple. However in future study, a complicated coupled interaction between the spar and float needs to be investigated.

In the first section we will discuss general forces acting on floating bodies. We will apply the principles to float, spar, and show heave response and compare the natural frequency of oscillation with high energy content energy spectrum. The analysis will be carried out for winter wave climate. Matlab scripts are listed in Appendix B, C.

5.2 Equilibrium of surface buoys

When a body is floating in water, a vertical force is applied through the center of gravity due to gravitational attraction called weight W_B. It acts vertically

downwards. The buoyancy is a vertical force applied opposite to weight through center of buoyancy. The buoyancy force is given by [22].

$$F_B = \iint p dA \tag{5.1}$$

The surface integral is evaluated over the immersed body. The tangential stress and normal stress results in friction and pressure on a moored buoy. The integration of friction and pressure stress gives hydrodynamic resistance. If the buoy is axis-symmetric then the only component in the direction of flow is applicable, drag [22, 23].

$$D_B = \frac{1}{2}\rho C_D A_N V^2 \tag{5.2}$$

Body Shape	Dimension ratio L /D	Drag coefficient C_D
Circular	1	0.63
Cylindrical	2	0.68
Axis perpendicular To flow	5	0.74

Table 5.1: Drag coefficient table [22]

The drag coefficient applicable to buoy with diameter of 4.5m and length 10m is 0.68.

5.3 Dynamics of buoy system

OWEC system heaving in waves consists of the spar system, damper, mooring, and buoy (float). Heave response study of OWEC system can be separated for buoy and spar. Also the coupled motion heave and roll can be studied separately. In the present study buoy heave response is studied alone. The buoy is coupled to spar, so there will be certain friction between buoy and spar. However the friction is neglected and analysis is separated for float and spar. In following section general transfer function is described.

The force required to move the buoy in water is given by [22],

$$F = (m + m')V \tag{5.3}$$

$$m_v = m + m' \tag{5.4}$$

$$m' = C_m \rho (Vol) \tag{5.5}$$

Where m' is added mass, m_v is called virtual mass, C_m is added mass coefficient, Vol is water displaced by the immersed body.

For calculating forces on the buoy, the assumption is made that the buoy dimensions are small as compared to wavelength i.e. buoy dimensions do not alter the wave shape. The assumption is made that downward forces are positive. The various forces acting on the buoy are given as follows:

Weight $W_B = \rho g S D$ acting downwards [22], (5.6)

Pressure a) Due to buoy displacement x z

$$P_1 = -\rho g S (D + X) \quad ` \tag{5.7}$$

b) Due to wave elevation η_0 [22]

$$P_2 = \rho g S \eta_0 e^{-KD'} \tag{5.8}$$

Applying Newton's second law of motion and balancing forces [22]

$$cx + bx' + m_v x'' = F_0 \cos(\omega t + \sigma) \tag{5.9}$$

$c = \rho g S$ = restoring constant

$b =$ Linear coefficient of heave damping

$d =$ Linear coefficient of wave induced drag.

Exciting force by waves is given by [22],

$$F_0 = A e^{-KD} \left[(c - m_v \omega^2)^2 + (d\omega)^2 \right]^{1/2} \tag{5.10}$$

The natural frequency of oscillation is given by,

$$f_n = \sqrt{\frac{m_v}{c}} \tag{5.11}$$

The drag forces can be linearised [22],

$$b = \frac{4}{3\pi}\omega\delta C_D S X$$

$$= \frac{4}{3\pi}\omega\delta C_D S A \tag{5.12}$$

By integrating the equation of motion, the equation of the heave motion is given by

$$x = \frac{A}{m_v}\frac{\left[(c - m_v\omega^2)^2 + (b\omega)^2\right]^{1/2}}{\left[(p^2 - \omega^2)^2 + 4n^2\omega^2\right]^{1/2}}\cos(\omega t + \sigma + \theta) \text{ [23]} \tag{5.13}$$

$$\theta = \tan^{-1}\left(\frac{-\omega b}{c - m_v\omega}\right)$$

θ is phase angle between force and the heave response.

The heave transfer function of the buoy is given by [23],

$$|H(\omega)| = \frac{\left[(c - m_v\omega^2)^2 + (b\omega)^2\right]^{1/2}}{\left[(p^2 - \omega^2)^2 + 4n^2\omega^2\right]^{1/2}} \tag{5.14}$$

5.4 Design of spar

The spar remains stationary with waves and does not freely move with waves as against the float. This produces relative linear motion between spar and float which produces useful energy. Over the useful range of energy spectrum, it can be observed from fig. 5.1 that the buoy does not heave in the frequency range of high energy content. This ideal behavior is obtained by heavily damping the spar by increasing damping coefficient. Also the damper plates provide damping to a bare pole (spar).

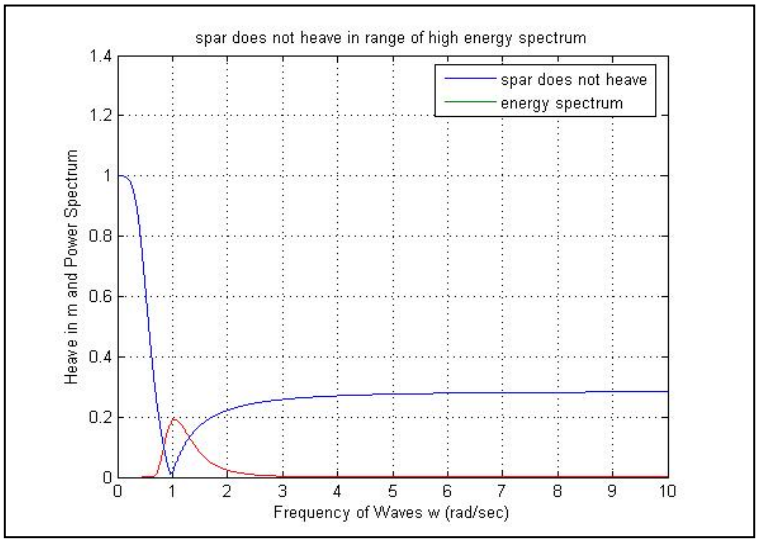

Figure 5.1 spar transfer function

The heave of spar rolls down to zero in frequency spectrum from 0.8 rad/s to 1.5 rad/sec. Most of the energy lies in this frequency range, there will be linear motion between spar and float. This will help to induce voltage in the coils. The

damper plates help to make the spar stationary. If a bare spar is deployed in sea, it would be unstable and jump out of water. Please refer to fig. 5.1 A good spar does not heave [22, 23]. A more detailed study of mooring design is left as a future work.

5.5 Design of buoy

The function of buoy is to follow ocean waves and produce relative motion between the float and spar. This can be observed over the frequency range of 0.8 rad/sec to 1.2 rad/sec. The heave response is high. The response will be limited by PTO damping coefficient. As most of the energy lies in this frequency range, it can be ensured that the dimensions of the buoy are helping in heave motion in the interested frequency range. Refer to fig. 5.2

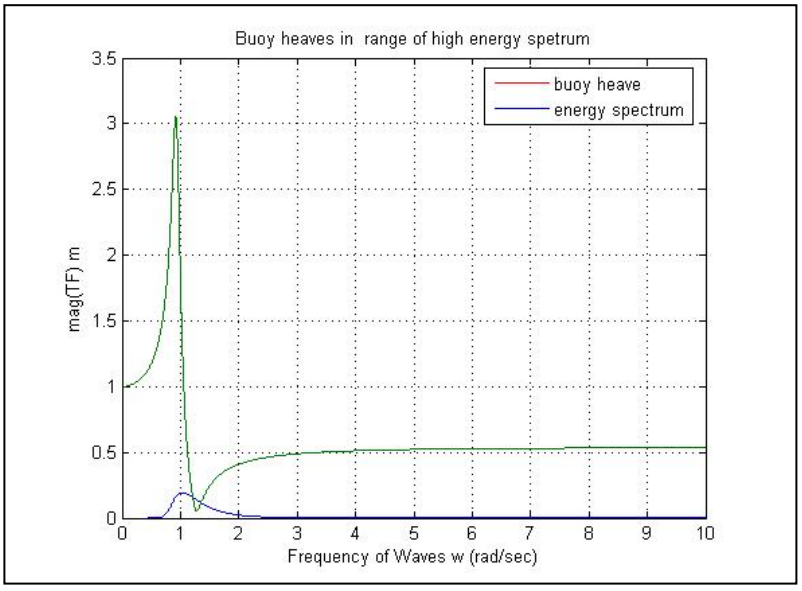

Figure 5.2 Buoy heave function

5.6 Wave energy spectral density

The Pierson-Markowitz spectrum is applicable to fully developed sea states. So a partially developed sea state which is not too restrictive and applicable to Oregon Coastal sites is selected. Such a spectrum is offered by the Bret Schneider spectrum. It is also called a two parameter spectrum [9, 24].

$$s(\omega) = 0.3125 * \frac{Hs^2 \omega^4}{\omega^5} * e^{-1.25(\omega s / \omega)^4} \tag{5.15}$$

$$\omega = \frac{2pi}{T_s}$$

H_s = Significant wave height (m)

T_s = Significant wave period (sec)

$$\int_{-\infty}^{\infty} s(\omega).d(\omega) = \left(\frac{Hs}{4}\right)^2 \tag{5.16}$$

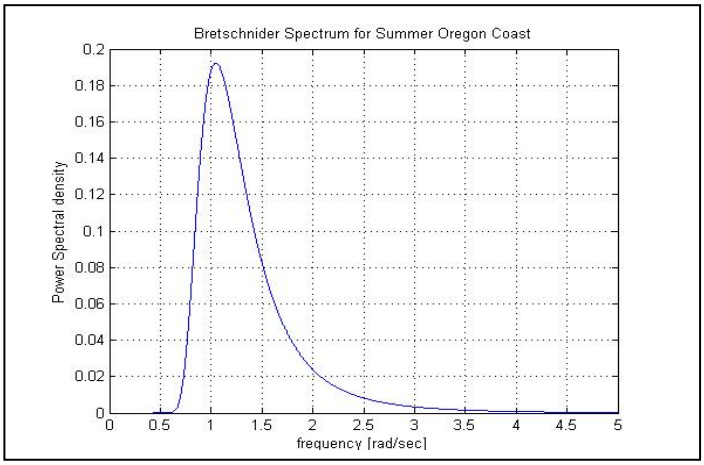

Figure 5.3 Energy spectrum

By varying frequency in equation (5.15), plot of energy spectrum is obtained. The frequency range for high energy content is noted for later on comparison with heave response.

6. CONCLUSIONS AND FURTHER WORK

6.1 Conclusions

A 100^{th} scaled model of ocean wave generator buoy systems is analyzed by solving the Navier-Stokes equations. These equations are numerically solved using CFD (Computational Fluid Dynamics) by implementing the front capturing method. Winter and summer wave climates are considered and the heave velocity of an oscillating buoy is studied in order to predict and to understand the power generated by the buoy. For verification of CFD results, a wave flume design from a dimensions perspective is presented. In addition, a 100^{th} scaled permanent magnet linear generator designed for high efficiency is presented.

The ocean buoy design is presented by drawing the transfer function in the heave motion. The frequency domain analysis is overlapped on the wave energy spectra for winter and summer conditions. MATLAB program scripts are listed for buoy dimensioning and linear generator design optimization. Also the linear generator design is verified using Maxwell-2D FEM code.

From simulations it was found that given the diameter of the ocean buoy of 4.5m, it can generate 35 kW rms power in winter, however the buoy can only generate 4 kW rms in summer with a damping factor of 0.25.

The optimized design of the PM linear generator designed using a 1mm air gap, with an efficiency of 96.5%, produces 2.2 W with a peak thrust of 30 N.

The damped frequency of heave motion is plotted and it is found that a 4.5m diameter buoy produces heave motion in the frequency range of the high energy spectrum. An entire design analysis of OWEC system and flume system is presented and verified by other methods.

6.2 Recommendations for Further Work

The CFD simulation provides power captured based on dimensions of the buoy, weight, PTO damping and wave climate. The buoy dimensions can be optimized with the help of MATLAB scripts. Please refer to Appendix C. The optimized dimensions can be integrated into CFD code to verify against wave flume results. Proper instrumentation provides reflected and transmitted wave amplitudes in the wave flume. These values need to be compared with CFD analysis to verify the accuracy of CFD codes and correction factors need to apply if any. The current scope of simulation is limited to a single buoy. An array of buoys can be simulated with the help of CFD. The interference free side by side distance and longitudinal distance needs to be verified using CFD codes. The flume experimentation can provide these values accurately which can be plugged into the CFD model. The CFD model helps to optimize parameters like buoy dimensions to obtain the maximum power. More advanced CFD simulation software like LSDYNA gives facility to model internal details of a PMLG. This is helpful to do stress analysis, vibration analysis of buoy.

The wave flume dimensioning is explained in chapter 3. A detailed analysis on physical properties, forces exerted by waves in scaled environment needs to be completed and is left as future work. Instrumentation forms a very important aspect of wave flume study. Many more projects are expected to be completed in coming years if a flume is built and kept ready with instrumentation.

The design of PMLG is explained in chapter 4. The assumptions made in the design were based on theoretical study and results obtained for other dimensions. The PMLG must be built practically. The operating conditions must be verified against assumed parameters in design. The effect of materials on PMLG efficiency is very critical.

Once the flume and PMLG is ready, the complete system needs to be tested against seasonal wave climates. The study will relate very important details like the load curve of the generator, regulation, stage efficiency in conversion etc. The study will also answer the best capacity factor and optimised dimensions of the machine under a given wave climate. In all, the scaled physical modelling forms a nice bridge between simulations and prototype, and forms a basic foundation towards the prototype designs.

One more strong focus on future work must be on optimum ocean wave energy control. Exact and efficient control of the ocean wave buoys/arrays will provide the ability to reliably and efficiently extract optimum power from the ocean. Since no control of this kind is in operation we have to start from scratch. With only limited investigation on buoy control we have already identified many aspects that must be more closely investigated before an efficient control scheme can be realized.

Having a ‘Sentinel Buoy’ upstream of the buoy array could provide us with near real-time information about the harmonic content of the existing wave conditions. Remember, however, that every wave frequency travels at different speeds in the ocean and all waves approach at different angles; therefore we cannot predict the actual wave profile at any great distance from the sentinel buoy.

The possibility of using a Doppler radar detector on the seafloor at every buoy could give us real-time wave profile information. This method could be able to accurately portray the buoys position and also the wave conditions so that the

controller could take the appropriate actions to achieve efficiency. This method would be very comprehensive but may prove too costly to employ.

Generator Tuning appears to be a big obstacle that must be addresses before an efficient control approach can be seen. In order to achieve a condition where the buoyant portion of the ocean wave converter moves at of near harmonic resonance with the incident waves we must have the ability to tune the device to the prominent wave frequency. This will be important in order to achieve maximum power output.

Generator tuning may be achieved in one of two regimes either mechanically or electrically. There are four parameters known to mechanical control engineers that can be adjusted to achieve desired mechanical tuning. These are mass, spring, damping and also the mechanical forcing function. Mass translates directly into the buoyancy of the wave generator and could potentially be adjusted dynamically with a water ballasting system. Spring could be achieved simply by adding a large mechanical spring into the system. Damping could be achieved with a shock absorbing device. The forcing function though always a function of the wave profile, can be drastically modified by the buoy design. For example large buoys would result in large amplitude forcing inputs.

A potentially more exciting and cost effective method of achieving generator tuning may be to employ electrical techniques. Mass for example may be simulated with a large inductive element on the terminals of the DC bus. Spring could be simulated with four quadrant control over the linear generator. Electrical damping will be the direct result of the power takeoff and can be achieved by altering the delay angle on the active rectifier.

Over damping may become a necessary option for these buoys for a variety of reasons. One reason is to protect the wave generator from exceeding its stroke and velocity limitations in larger than normal wave conditions. This means we must

investigate whether the generator must be built oversized to achieve these damping values or should we incorporate a mechanical damper in the system.

Additional work should be considered in the physical layout of the linear generating device. The organization of the permanent magnets, copper, and iron has only lightly been explored. Investigation into the most efficient organization in terms of cost, efficiency, materials and weight could lead to drastically more viable linear generators.

BIBLIOGRAPHY

[1] Renewable energy an overview, March 2001, DOE/GO-102001-1102. http://www.nerl.gov/docs/fy01osti/27955.pdf

[2] Teresa Hansen, "*Catching a Wave*", *Power Engineering.*

[3] M.E. McCormick, "*Ocean Wave Energy Conversion*", *Wiley,* 1981.

[4] Technology White paper on Wave Energy Potential on the U.S Outer Continental Shelf., http://ocsenergy.anl.gov

[5] S. Ragunathan, "*A methodology for Well's turbine design for wave energy conversion*," Proc. IMechE*,* vol. 209, pp. 221-232, 1995.

[6] Energetech; http://www.energetech.com.au/

[7] H.C Soerensen, L.K Hansen and R. Hansen, "*Environmental impact, European Thematic Network on Wave Energy*", tech. report NNE5-1999-00438 WP 3.3., Jan 2003

[8] Nasar S.A, "*Linear Electric actuators and generator*". Cambridge university press: 2005.

[9] S. K. Chakrabati, "*Hydrodynamics of Offshore Structures*" Springer Verlag, 1987.

[10] Shaw R, " *Wave Energy A design challenge*", Ellis Horwood Publishers

[11] Lighthill J, "*Waves in fluids*", Cambridge university press, 1978

[12] Currie, I.G, "*Fundamental mechanics of fluids*", Mc-Graw-Hill, 1993.

[13] M.E. McCormick, "*Ocean Engineering Wave Mechanics"*, Wiley, 1973.

[14] E.B. Agamloh, A.K. Wallace, A. von Jouanne, "*A novel wave energy extraction device with contact less force transmission system*," *44th AIAA Aerospace Sciences Meeting,* Reno, Nevada, Jan 2006.

[15] R. G. Dean and R.A. Dalrymple,"*Water Wave mechanics for Engineers and Scientists*", Englewood Cliffs: Prentice-Hall, Inc., ISBN 0-13-946038-1, 1984.

[16] Rotterdam: A. A *,"Physical modeling in Coastal Engineering"*, Balkema, Inc., ISBN 90-6191-516-3, 1985.

[17] J.Falnes, "*Ocean Waves and oscillating systems*", Cambridge University Press, 2002.

[18] P.V.Shotri, "*Fluid mechanics*", Nirali Prakashan, India, 2004.

[19] http://www.chc.nrc.ca/English/Lab%20Tech/LabTech_AWA_e.html

[20] Oskar Danielson, et.al. Permanent magnet fixation concepts for linear generator. University of Uppsala, Sweden.

[21] Hamzah Arof, A. Eid et.al 2004. Permanent magnet linear generator design using Finite Element Modeling. IEEE 2004, 0-7803-8575-6/04

[22] Henri O. Berteaux., Coastal and Oceanic buoy engineering, Gulf Publishing Corporation

[23] H.O Berteaux., Buoy Engineering A Wiley-inter science publication.

[24] M. E. McCormick, "Ocean wave energy conversion concepts," *IEEE OCEANS*, vol. 11, pp. 553-558, 1979.

BIBLIOGRAPHY FOR IMAGES

[1.1] Ocean Power Delivery Limited, *http://www.oceanpd.com/Pelamis/default.html*

[1.2] Energetech Australia Pty Ltd, *http://www.energetech.com.au*

[1.3] Wave Dragon Aps, *http://www.wavedragon.ne/*

[1.4] AWS Ocean Energy Limited, *http://www.waveswing.com/*

[1.5] AquaEnergy Group Ltd, *http://www.aquaenergygroup.com/*

[1.6] Oregon State University, *http://eecs.oregonstate.edu/msrf/*

[1.7] Oregon State University, *http://eecs.oregonstate.edu/msrf/*

[3.5] SonTek/YSI, *http://www.sontek.com/apps/flume/adv-swf/adv-swf.htm*

[3.6] eFunda Inc, *http://www.efunda.com/designstandards/sensors/laser_doppler /laser_doppler_intro.cfm*

APPENDICES

A. MATLAB CODE FOR PMLG DESIGN

```
clc;
clear all;

%Design of Linear Generator %

%*********Constants in the system ***********8
Mui = 200; % assumed relative permeability of iron
Mu0 = 4*pi*(10)^-7;
Mum = 1.13*Mu0;
H = 38000;
sigmai = 5 * (10^6);
Br  =  1.02;
Hc = 0.7;
Bg = 0.6; % the reason for choosing low value of Br and Bg is to
avoid saturation
Bsc = 1.37 ; % back iron flux density
Ks = 1 ; % saturation and additional air gap for laminations
rhoAv = 7 * (10^3); % The density of iron
rhoRes = 2.3 * (10^-8);
%********* Design Specifications  **********
Dse = 0.047; % external diameter of Float
gacc = 9.81 ; % acceleration  due to  gravity
Drod = 18/1000 ; % diameter of spar
Slength = 0.035; % Stroke length of Waves for Winter
Ulinear = 0.2749 ;% linear speed of Generator


acc = 0.2; % reverse acceleration
g = 1/1000; % air gap
K1 = 0.1 ; % loss coefficient in the tooth. Find its Value
Btooth = 1.37; % assume value of Btooth or take from Simulation
hsi = 1*(10^-3); % Why to assume value of hsi = 1mm
% Mode of operation is Oscillator
%Enviornment is Corrosive
Thrust = 5; % in N for continous duty
%Im = 0.5;
Nc = 50;
%Nc = [10 20 30 40 50 60 70 80 90 100];

Ns = 1 ; % What is Ns not clear ????/?
p = 4; %pole pair
%********Magnetic Circuit Design ***********
%Tubular design , ring shaped design
Tau = 0.03; % pole pitch is assumed as 3 cm
%Taup = (5/6) * Tau; %
```

```
f1 = Ulinear/(2*Tau);  % f1 is fundamental frequency and Tau is
pole pitch
t1 = Slength./Ulinear; %t1 = travel time = Stroke Length / Linear
Speed
Numperiod = round(t1.*f1);  % calculate total no of periods for
travel time
Kfill = 0.75; % slot filling factor
%Current and flux in machine required for 1 period to travel along
the
%stroke length
w = 2 * pi * f1;
Diron  = sqrt(2./(Mui.*w.*sigmai));

%Tauslot = Tau/2;
Tauslot = 2*Tau/3;
ts = Tauslot/2 ;
% ts = 0.015;
Taup = Tauslot - ts;
Gamma = (ts/g)^2/(5+(ts/g));
Kc = 1/(1-(Gamma*g/Tauslot)); % Carter Coefficient

% Demagnetisation Characteristics of PM
Hhm = -Bg/Mu0 * (Kc * g *(1+Ks)); % Product of Hm * hm..magnet ring
height
Hm = (Bg - 1) / (Mum );
hm = round(Hhm/Hm*1000)/1000;
%hm = 0.0080;

%Calculation of Magnetic Air gap Gm
a = Mu0 *(hm/Mum);
Gm = round((Mu0 *(hm/Mum) + (g*Kc* (1+Ks)))*1000)/1000;

% Calculation of Slot Depth
Dsi = Drod  + (2*hm) +(2*g); % Why  2* hm is added as hm is height
of ring ???? This is internal diameter of Float
% Let hs = slot height and hsc = back iron thickness and Sums = hs
+ hsc
Sumh = (Dse - Dsi) /2;
hsc = Bg/Bsc*(Taup/2);

% more correct value of hsc is hscnew
hscnew = hsc * (Dsi/(Dse - hsc));
hsu = round(((Sumh) - hscnew - (0.94/1000))*1000)/1000; % 0.94 mm
remain unfilled
% hsu = 0.0030;
% ts = 0.0050;

Jcomax = 2e+005;
%Jcomax = 1.1111e+004;
```

```
Im = (Jcomax*hsu*ts*Kfill)/Nc
Jcorms = sqrt(2/3) * Jcomax;
%hsu = 0.0070;

hs  = Sumh - hscnew;
% check on Flux density  in the rotor rod
Bcr = 4*Taup/2*(Drod+hm) * Bg/(Drod^2);
Mur = Bcr / (H*Mu0);

Fxp = Bg * 2* Nc * Im * (pi * Dsi) * (2*p) ;

% Caluclate the moving weight
m = 2*(pi/4) * (Drod + 2*hm)^2 * rhoAv*2*p*Tau;
%(2*p) * Tau * rhoAv;
Fdynamic = 2*acc*m; % a needs to be changed
% Caluclate the moving weight
Hproduct = (Drod+2*hm)^2;
%m = 2*(pi/4) * (Drod + 2*(hm).)^2 * (2*p) * Tau * rhoAv;
%m =1;
%Fdynamic = 2*acc*m; % a needs to be changed



%after balancing equation of forces
% product of Nc * Im = NcIm assuming Fthrust = 5 N
Fthrust = Fxp - (Fdynamic+(gacc*m)); % thrust is little bit low
than calculated ?????
%Jcomax = (Nc * Im)/(hsu * ts * Kfill);
% Nc=50;
% Im=0.5;
%Thrust and Stator slot mmf Calculations
Fxp = Bg * 2* Nc * Im * (pi * Dsi) * (2*p) ;


% Losses Calculation
% Core losses in the tooth are
Pct  = 96 * K1 * (f1^2) * (Btooth^2);
Vct = pi/4*((Dsi+2*hs)^2-(Dsi^2))*(Tau-ts);
Pct_total = Pct * Vct;

% Core losses in  the Core are

Pc = 32*K1*(Tau/Taup) *(f1^2) * (Br^2); % Here Bccs is assumed to
beequal to Br Check from Simulation
Vc = pi/4*((Dse)^2-((Dsi+2*hs)^2))*Tau;
Pc_total = Pc * Vc;
%Jcomax = 1.85*(10^6);
Coreloss = Pct_total + Pc_total;
```

```
%Parameters are function of number of Conductors
Rs = rhoRes * pi * (Dsi + hs) * (Jcomax) * Ns * (2*p) * (Nc) *
(Nc)/(Im*Nc);
Lssigma = Mu0 * Nc* Nc * (2*p) * (Dsi+hs) * ((hsu/3*ts) + (hsi
/ts));
Lm = 6*Mu0/(pi*pi) * (Nc * p)^2 * (Tau * pi * Dsi) /(p * Gm);
Ls = Lssigma + Lm;

% Calculation of Time constant Taue

Taue = Ls / Rs;

%Motion line Voltage
% t=0:0.01:1; % time
% waves = (0.35/2)*(2*pi/0.8)*cos((2*pi/0.8)*t); % winter season
% %Ulinear = 0.2*(0.35/2)*(2*pi/0.8)*cos((2*pi/0.8*(t-0.01))+90); %
efficiency of waves to linear speed 20%
% Ulinear = 0.2*(0.35/2)*(2*pi/0.8)*cos((2*pi/0.8*(t)));

%Ulinear1 = 0.2*(0.35/2)*(2*pi/0.8)*cos((2*pi/0.8*(t-0.01))+90);
% delay of 10 ms from waves to  float
%Bg = 0.3;
%El = 0.9*Bg * Ulinear * (pi * Dsi ) * ( 2* p)  * ( 2 * Nc)
El = 1*Bg * Ulinear * (pi * Dsi ) * ( 2* p)  * ( 2 * Nc)
% Caluclate Wire Size
Aco = Im /(Jcomax);
dco = sqrt(4/(pi) * Aco); % this value is in m
dcomm = dco * 1000;

Copperloss = Im^2 * Rs;
Totaloss = Coreloss + Copperloss;
%Caluclation of Peak  Thrust Density

% Peak thrust is given  by

Fpk = Fdynamic + (m*gacc) + Fthrust;

% peak thrust density
% Fpk = 25;
% p=1;
fpk = Fpk /((pi)*(Drod + (2*hm)) *(2*p) *(Tau))*(10^-4); % This
value is in N/(cm^2)
% Rl = 1;
% Output = El.*Im;

Copperloss = Im^2 * (Rs);
Totaloss = Coreloss + Copperloss;
% % Output = Totaloss/(1-(Eff/100));
% % Im = Output/El;
```

```
% %Vary speed and check Output Voltage Plot Characteristics
% % Calculate Efficiency and Load Characteristics by taking
excternal circuit
% % into account Plot the load and Efficency Characteristics
% %Cogging Force Calculations and Plot Characteristics
%
% i=sqrt(-1);
% %(i*w*Ls)
% %Im = 0.2;
% Vout = El-((Rs+Rl+(i*w*Ls))*Im);
% Voutmag = abs(Vout);
% %Im = Output/Voutmag;
% Pout = Voutmag*Im;
%
%
%


j = sqrt(-1);
Xs = j*w * Ls;
Rl = Rs+Xs;
Rl = 20;
den = 1+((Rs+Xs)/Rl);

Vout = abs(El/den);
I=  Vout/Rl;

Pout = Vout*I;
 Output = real(Pout);
Copperloss = I^2 * (Rs);
Totaloss = real(Coreloss + Copperloss);
Eff = (Output./(Output+Totaloss)).*100

% plot(t,waves,t,Ulinear,'r',t,El,'g');
% ylabel('Emf, celerity of waves, PMLG velocity');
% legend('Ocean Waves','PMLG speed','Emf generated');
% title('Emf generation from Waves');
```

B. MATLAB CODE FOR BUOY DESIGN

```
% Heave Dynamics of Buoy Heaving in Ocean Waves %

% ************General Constants***********
g = 9.81;  %acceleration due to graqvity
rhoWater = 1025 ; % density of sea water
Cd = 0.68 % drag coefficient of Cylinder Bertiaux page 39
A = 0.2;
D= 5; % draft  below water
%Hs = 3.5; %significant wave height Summer Run this simulation for
Winter Hs = 2.5
%Ts = 8; % for Winter Ts = 8

 Hs = 1.5; %significant wave height Summer Run this simulation for
Winter Hs = 2.5
 Ts = 6; % for Winter Ts = 8

%***********Dimensions of Buoy ***********
Dspar = 0;
Lspar = 0;
Dfloat = 4.5;
Lfloat = 10;
Ddamper = 0;
Ldamper = 0;
% Dfloat = 0.6;
% Lfloat = 6.7;


%  Ddamper = 15.5;
%  Ldamper = 0.5;


%**********Calculation of Areas ***************
Aspar = pi/4*(Dspar^2);
Afloat = pi/4*(Dfloat^2);
Adamper = pi/4*(Ddamper^2);
% 1 is top surface area and 2 is bottom surface area
Sf1 = 2*pi/4*(Dfloat^2-Dspar^2);
%Sd1 = pi/4*(Ddamper^2-Dspar^2);
%Sd2 = pi/4*(Ddamper)^2;
%S = 1.5/3*(Sf1+Sd1+Sd2);
 S = 1*(Sf1);
 %+Sd1+Sd2);
%*************Calculation of Mass *****************
%mass = density * volume = density * (area * length)
```

```
Mbasic  = rhoWater *((Aspar * Lspar) + (Afloat * Lfloat) +
(Adamper* Ldamper));
Madded   = rhoWater * 1.333* pi*((Dfloat/2)^3+
(Dspar/2)^3+(Ddamper/2)^3);
Mtotal = Mbasic + Madded; % 216 Kg


%Frequency bins for plotting ***
w = (0.0001 : 0.0001 : 10);
Xestimate = 0.25; % heave estimate of buoy

%**********Force Balacnce Equation Constants **********
%b = linear coefficient of Heave damping  + PTO damping
%b = 0.8*8/(3*pi)*(rhoWater*Cd*S) * (w).*Hs; % winter
%b = 5.8*8/(3*pi)*(rhoWater*Cd*S) * (w).*Hs; %Summer
%damping is 4 times hydrodynamic damping
b = 1*(4/(3*pi))*(rhoWater*Cd*S) * (w).*Hs; %Summer
b = b + 4*b;
%b = b+ 10.75;
%b=0.25e-10;
%d = linear Coefficient of Wave induced Drag
d = (4/(3*pi)) * (w * rhoWater * Cd * S); % neglecting Spar
%c = restoring constant
c = rhoWater * g * Afloat;
%c = rhoWater*g*Afloat;
p=sqrt(c/Mtotal); %undamped frequency ofoscillation
n = b/(2*Mtotal);
% Buoy RAO aka Transfer function ( Response Heave Amplitude RAO)
%numPartA = (c-(Mtotal * (w.^2))).^2;
numPartA = (c-(Madded * (w.^2))).^2;
numPartB = (d.^2).*(w.^2);
%denPartA = (c-(Mtotal * (w.^2))).^2;
denPartA = (p^2-(w.^2)).^2;
%denPartB = (b.^2).*(w.^2);
denPartB = 4*(n.^2).*(w.^2);
num = sqrt(numPartA + numPartB);
%num = Hs*(2*rhoWater*((g^3)./w.^3).*b).^(1/2);
%num = (2*rhoWater*(g^3)./(w.).^3*(b.))^(1/Hs);
den = sqrt(denPartA + denPartB);
%num = ((c-(Mtotal*(w.^2))).^2 + (d^2).*(w.^2)).^0.5;

%den = ((c-(Mtotal*(w.^2)).^2) + ((b^2).*(w.^2))).^0.5;
Htf = num./(den*Mtotal*Hs);



%*******Spectrum for Waves ******
ws = 2*pi/Ts;
PspartA = exp(-1.25*(ws./w).^4);
```

```
Pspectrum = (1.25/4)*Hs^2*((ws^4)./(w.^5)).*PspartA;

plot(w,Pspectrum,'b',w,abs(Htf),'r');
legend('Power Spectrum','Transfer function buoy');

title('Power spectrum and heave transfer function : Winter');
hold on
xlabel('Frequency of Waves w (rad/sec)');
ylabel('Heave in m and Power Spectrum in W');


grid;
```

C. MATLAB CODE FOR SPAR DESIGN

```
% Heave Dynamics of Spar Heaving in Ocean Waves %

% ************General Constants***********
g = 9.81;  %acceleration due to graqvity
rhoWater = 1025 ; % density of sea water
Cd = 0.68 % drag coefficient of Cylinder Bertiaux page 39
A = 0.2;
D= 5; % draft  below water
%Hs = 3.5; %significant wave height Summer Run this simulation for
Winter Hs = 2.5
%Ts = 8; % for Winter Ts = 8

 Hs = 1.5; %significant wave height Summer Run this simulation for
Winter Hs = 2.5
 Ts = 6; % for Winter Ts = 8

%***********Dimensions of Buoy ***********
Dspar = 0;
Lspar = 0;
Dfloat = 0.09;
Lfloat = 80;
Ddamper = 0;
Ldamper = 0;


  Ddamper = 15.5;
  Ldamper = 0.05;


%**********Calculation of Areas ***************
Aspar = pi/4*(Dspar^2);
Afloat = pi/4*(Dfloat^2);
Adamper = 1*pi/4*(Ddamper^2);
% 1 is top surface area and 2 is bottom surface area
Sf1 = 2*pi/4*(Dfloat^2-Dspar^2);
Sd1 = 1*pi/4*(Ddamper^2-Dspar^2);
Sd2 = 1*pi/4*(Ddamper)^2;
%S = 1.5/3*(Sf1+Sd1+Sd2);
 S = (Sf1+Sd1+Sd2);
%*************Calculation of Mass *****************
%mass = density * volume = density * (area * length)
Mbasic  = rhoWater *((Aspar * Lspar) + (Afloat * Lfloat) +
(Adamper* Ldamper));
Madded   = 1*0.25*rhoWater * 1.333* pi*((Dfloat)^3+
(Dspar)^3+(Ddamper)^3);
```

```
Mtotal = Mbasic + Madded; % 216 Kg


%Frequency bins for plotting ***
w = (0.0001 : 0.0001 : 10);
Xestimate = 0.25; % heave estimate of buoy

%**********Force Balacnce Equation Constants **********
%b = linear coefficient of Heave damping  + PTO damping
b = 8/(3*pi)*(rhoWater*Cd*S) * (w).*Hs*40;
%b=0.25e-10;
%d = linear Coefficient of Wave induced Drag
d = (4*1/(3*pi)) * (w * rhoWater * Cd * S);
%(Afloat+Adamper)); % neglecting Spar
%c = restoring constant
c = rhoWater * g * S;
%c = rhoWater*g*Afloat;
p=sqrt(c/Mtotal); %undamped frequency ofoscillation
n = b/(2*Mtotal);
% Buoy RAO aka Transfer function ( Response Heave Amplitude RAO)
%numPartA = (c-(Mtotal * (w.^2))).^2;
numPartA = (c-(Madded * (w.^2))).^2;
numPartB = (d.^2).*(w.^2);
%denPartA = (c-(Mtotal * (w.^2))).^2;
denPartA = (p^2-(w.^2)).^2;
%denPartB = (b.^2).*(w.^2);
denPartB = 4*(n.^2).*(w.^2);
num = sqrt(numPartA + numPartB);
%num = Hs*(2*rhoWater*((g^3)./w.^3).*b).^(1/2);
%num = (2*rhoWater*(g^3)./(w.).^3*(b.))^(1/Hs);
den = sqrt(denPartA + denPartB);


%den = ((c-(Mtotal*(w.^2)).^2) + ((b^2).*(w.^2))).^0.5;
Htf = num./(den*Mtotal);


% heave profile
XpartA = A * exp(-((w.^2).*D)./g).*abs(Htf);
theta = atan((-w.*b)/(c-Mtotal*(w.^2)));
XpartC = cos(w +(pi/2)+theta); % sigma = pi/2 ensures resonance of
buoy with waves
x = XpartA.* XpartC;
% subplot(3, 3,1);
% plot(w,abs(Htf));
% hold on
% xlabel('Frequency of Waves w (rad/sec)');
% ylabel('mag(TF) m');
```

```
% subplot(3 , 3, 2);
% plot(w,abs(x));
% hold on
% xlabel('Frequency of Waves w (rad/sec)');
% ylabel('Heave in m');


%*******Spectrum for Waves ******
ws = 2*pi/Ts;
PspartA = exp(-1.25*(ws./w).^4);
Pspectrum = (1.25/4)*Hs^2*((ws^4)./(w.^5)).*PspartA;
% subplot(3 , 3, 3);
plot(w/(2*pi),Pspectrum,'r',w/(2*pi),abs(Htf),'b');
legend('Power Spectrum','Spar tf');
hold on
xlabel('Frequency of Waves w (rad/sec)');
ylabel('Heave in m and Power Spectrum');
title('Spar profile in summer');
grid;
```

APPENDIX D

Wave Energy and Power

The total energy per unit width of a wave is given by sum of the potential and kinetic energy. Their average values over one wave length are given by [4]

$$PE_{av} = \int_0^{\lambda} \frac{\rho g \eta^2}{2} dx = \int_0^{\lambda} \rho g H^2 \sin^2(kx - \omega t) dx = \frac{\rho g H^2 \lambda}{16} \quad \text{(D.1)}$$

Kinetic energy per unit width, [3],

$$KE_{av} = \frac{\rho}{2} \int_0^{\lambda} \int_{-h}^{g} (u^2 + v^2) dx dz = \frac{\rho g H^2 \lambda}{16} \quad \text{(D.2)}$$

Total energy per unit surface area [4],

$$E_{av} = PE_{av} + KE_{av} = \frac{\rho g H^2 \lambda}{8} \quad \text{(D.3)}$$

The forces exerted by waves on floating or submerged bodies per unit width is given by [10]

$$F = \frac{1}{4} \rho g (a_i^2 + a_r^2 - a_t^2)(1 + \frac{2kh}{\sinh kh})$$

Where a_i (incident), a_r (reflected), a_t (transmitted) wave amplitude.

$$F = \frac{1}{4} \rho g (a_i^2 + a_r^2 - a_t^2) \quad (h -> \infty \text{ for deep water}) \quad \text{(D.4)}$$

The wave length for deep water waves is given by [3],

$$\lambda = \frac{g T^2}{2\pi} \quad \text{(D.5)}$$

Substituting equation (D.5) into equation (D.3) , incident wave power in deep sea expressed in [W/m] of crest length is given by

$$P_w = \frac{\rho g^2 T H^2}{32\pi} \tag{D.6}$$

APPENDIX E

1/100th scaled modeling.

In this section we explain why 1/100th scaled modeling is used. The actual buoy diameter is 4.5 m. To build this prototype and test it, would be expensive without verifying its functionality. Therefore, CFD modeling is considered to understand fluid-solid interaction. Currently available CFD programs do not support full scale modeling. However, even if there is a CFD model which supports full scale modeling, questions remain regarding reliability.

The alternative is to model scaled down version which is cheap to built and also helpful to verify the CFD accuracy. If CFD models are verified using wave flume results then we are confident about the CFD results.

Once the models are verified, we can scale the dimensions for prototype building.